Full title

Epithelial microinvasion and immunity elicited by disease-attenuated pneumococcal biosynthesis gene mutants

Running title

Epithelial microinvasion, immunity and disease

Caroline M. Weight[1*], Gabriele Pollara[1], Modupeh Betts[1], Roberta Ragazzini[2], Elisa Ramos-Sevillano[3], Jesús Reiné[4], Matthew Whelan[1], José Afonso Guerra-Assunção[1], Michael Connor[5], Paola Bonfanti[1,2], Clare Jolly[1], Mahdad Noursadeghi[1], Daniela M. Ferreira[4], Jeremy S. Brown[3], Robert S. Heyderman[1]

[1]Research Department of Infection, Division of Infection and Immunity, UCL London, UK

[2]Francis Crick Institute, London, UK

[3]Department of Respiratory Medicine, UCL, London, UK

[4]Oxford Vaccine Group, University of Oxford, Oxford and Clinical Sciences, Liverpool School of Tropical Medicine, Liverpool, UK

[5]Chromatin and Infection, Institut Pasteur, France

*Current address Biomedical and Life Sciences, Faculty of Health and Medicine, Lancaster University, UK

Corresponding Authors: Dr Caroline M. Weight and Professor Robert S. Heyderman

Email: c.weight@lancaster.ac.uk and r.heyderman@ucl.ac.uk

ABSTRACT

Nasopharyngeal colonisation by *Streptococcus pneumoniae* is characterised by adherence to epithelial cells, microinvasion and an innate immune response. Here, we explore the hypothesis that pneumococcal virulence has primarily evolved to promote these colonisation processes and subsequent transmission, rather than to cause disease. We have used a *S. pneumoniae* serotype 6B strain, alongside two biosynthesis gene mutants (Δ*proABC* and Δ*fhs* with an additional Δ*piaA* mutation) known to colonise murine and human models without causing disease. We show that these mutations do not attenuate microinvasion in either experimental human pneumococcal challenge or *in vitro* in primary and immortalised epithelial cells. However, interactions and subsequent cellular reorganisation by primary human airway epithelial and Detroit 562 nasopharyngeal cells were strain dependent, and the inflammatory epithelial innate response and caspase 8 activity were attenuated by the Δ*fhs/piaA* but not the Δ*proABC/piaA* mutation. Growth of the Δ*fhs/piaA* mutant was associated with increased pneumococcal hydrogen peroxide secretion and reduced pneumolysin activity when compared to the WT and Δ*proABC/piaA* mutant strains. Analysis of the bacterial transcriptome under stress conditions revealed that the mutations resulted in broad, differential effects on pneumococcal virulence and metabolic gene expression suggestive of compensatory changes that preserve microinvasion. The findings that cellular reorganisation, the innate immune response, and the ability to cause invasive disease are not necessarily interconnected emphasise the complexity of bacterial-host interactions at the mucosal surface. Colonisation outcome cannot be fully explained by single or functionally grouped virulence or metabolic factors.

IMPORTANCE

Colonization of the nasopharynx by *Streptococcus pneumoniae* is a precursor to both disease and bacterial transmission. This study challenges the assumption that virulence factors have primarily evolved to cause disease, proposing instead that these pathogenic factors more aligned with facilitating bacterial carriage and spread. Using a pneumococcal clinical isolate strain and two biosynthesis gene mutants in experimental human pneumococcal challenge and epithelial cell line

models, we demonstrate that epithelial microinvasion can occur independently of disease causation. Moreover, we uncover a complex relationship between bacterial adaptation and epithelial immune response, with differential effects on epithelial cell reorganization, inflammation, and bacterial growth dynamics. Our findings underscore our contention that pneumococcal colonisation and disease outcomes cannot be predicted by individual gene profiles alone. This phenotyping approach offers the opportunity to effectively unravel *S. pneumoniae* pathogenesis and its adaptation to the nasopharyngeal niche.

Keywords

Biosynthesis genes, host-pathogen interactions, Innate immunity, *Streptococcus pneumoniae*, airway epithelium

Graphical Abstract

S. pneumoniae colonisation is characterised by mucus association, epithelial adherence and microinvasion – where the pneumococcus invades the epithelial barrier without causing disease. Microcolonies form at the epithelial surface and pneumococcal transmigration can occur between epithelial cells. Although mutations in *S. pneumoniae* biosynthesis genes (Δ*proABC* and Δ*fhs*) attenuate disease in a murine model, they do not attenuate microinvasion in either experimental human pneumococcal challenge (EHPC) or *in vitro* in primary and immortalised epithelial cells. These mutations show strain-dependent effects on both the epithelial and bacterial responses to infection. While not directly co-correlated, factors such as epithelial cellular reorganisation, inflammation and caspase 8 activity alongside pneumococcal metabolic adaptation, virulence factor expression and response to stress are key determinants of the outcome of colonisation in the nasopharyngeal niche.

INTRODUCTION

Adaptation to the host environment is crucial for successful colonisation of the upper respiratory tract (URT) by a range of human pathogens, including bacteria, viruses and fungi. This includes the ability to withstand different ambient temperatures, overcome physical barriers such as mucus, evade epithelial soluble mediators such as antimicrobial peptides, compete with neighbouring polymicrobial communities and compensate for nutrient restriction (1). *Streptococcus pneumoniae* (the pneumococcus) is a common commensal of this URT niche (1). However, translocation of the pneumococcus from the nasopharynx to the lungs, blood or the brain results in life-threatening disease (1). Indeed, among children under five years, *S. pneumoniae* is the leading cause of pneumonia deaths globally (2).

Using experimental human pneumococcal challenge (EHPC) of healthy volunteers and well-characterised epithelial cell models, we have previously shown that colonisation by *S. pneumoniae* is characterised by epithelial surface microcolony formation and invasion which we have called microinvasion (i.e. invasion of the epithelial barrier without disease) (3). The pneumococcal capsule is a major virulence determinant, influencing carriage, transmission from person to person, and invasive disease potential (4). Indeed, we have shown that *S. pneumoniae* epithelial microinvasion also varies markedly between strains expressing different capsular serotypes, with a serotype 4 strain invading Detroit 562 nasopharyngeal cell monolayers more readily than serotype 6B and 23F strains, and inducing more marked pro-inflammatory epithelial transcriptomic and cytokine responses (3).

We and others have previously proposed that although the epithelial innate immune response that results from pneumococcal colonisation may facilitate clearance, this highly variable pathobiont (>100 serotypes; >600 global pneumococcal sequence clusters (5)) tunes the host response to enhance transmission(3, 4). In addition to capsule, these processes have been shown to be

105 modulated by a broad array of subcapsular and cytoplasmic virulence factors (6), and more recently,
106 by bacterial carbohydrate, nucleotide, fatty acid and purine/ pyrimidine metabolism (7-11).

107

108 To explore the hypothesis that pneumococcal virulence has primarily evolved to promote
109 colonisation and subsequent transmission, but not necessarily disease, we have used a unique set
110 of *S. pneumoniae* serotype 6B Δ*proABC* and Δ*fhs* biosynthesis gene mutants developed to induce
111 protective immunity without causing disease (12). *proABC* and *fhs* were chosen as targets through
112 the analysis of previously published transcriptome and transposon mutational screens (11, 13, 14).
113 The *proABC* operon, consisting of genes predicted to encode a γ-glutamyl phosphate reductase
114 (*proA*), a γ-glutamyl kinase (*proB*) and a pyrroline-5-carboxylate reductase (*proC*), and *fhs* predicted
115 to encode a folate tetrahydrofolate reductase involved in one carbon metabolism pathways have
116 been implicated in metabolic adaptation to growth (15-17), and are highly transcribed in mouse
117 models of pneumococcal infection (16, 17). To further avoid reversion to a disease-causing
118 phenotype during EHPC, these mutants also contain a deletion of *piaA* which encodes the lipoprotein
119 component of the dominant pneumococcal iron uptake ABC transporter (18, 19). We have previously
120 shown that in a murine model, when compared to the *S. pneumoniae* serotype 6B wild-type parent
121 strain (WT, BHN418), the Δ*proABC/piaA* and Δ*fhs/piaA* mutants colonise the nasopharynx as
122 effectively. However, despite expressing the same capsule as the wild type 6B strain, neither the
123 Δ*proABC/piaA* and Δ*fhs/piaA* 6B strains causes invasive disease (12) (17). We have subsequently
124 shown that this attenuated phenotype is at least in part due to impaired growth in serum and is
125 associated with increased oxidative stress and altered lipid profiles (17). In EHPC, we have also
126 shown that both Δ*proABC/piaA* and Δ*fhs/piaA* retain the ability to colonise the human host, and can
127 induce IgG-mediated immunity (20). Therefore, these otherwise isogenic strains allow us to compare
128 the pneumococcal-epithelial interactions of disease-causing and non-disease-causing phenotypes,
129 while avoiding the confounding of differences in capsular serotype.

130

131 Here, we reveal that although the *S. pneumoniae* Δ*proABC/piaA* and Δ*fhs/piaA* metabolic function
132 mutations result in disease attenuation, the ability of the mutant strains to colonise and cause
133 microinvasion in both EHPC and *in vitro* epithelial infection models is preserved. Crucially, we also
134 show that despite similar patterns of epithelial cellular engagement, disruption of these key
135 pneumococcal metabolic pathways has differential effects on cellular reorganisation and innate
136 responses, which we propose influences niche adaptation during colonisation.

137

138 **RESULTS**

139

140 ***S. pneumoniae* 6B with Δ*proABC* or Δ*fhs* mutants colonise in EHPC with evidence of epithelial**
141 **microinvasion**

142 We have defined microinvasion as the process by which *S. pneumoniae* invades the mucosal
143 epithelium, inducing an innate immune response, without necessarily causing disease (Fig 1A).
144 Nasal curette samples from EHPC healthy volunteers inoculated with the *S. pneumoniae* serotype
145 6B WT or isogenic mutant strains *(*Δ*proABC/piaA* or Δ*fhs/piaA*) (21) were collected to investigate the
146 extent of epithelial association and microinvasion. A positive carrier was defined as colonisation at
147 any time point (day 2 or day 6 post-inoculation), as detected by microbiology culture (3). Visualisation
148 of the mucosal cells by confocal microscopy showed colonisation by the WT and mutant
149 pneumococcal strains (Fig 1B). At day 6 post challenge, compared to WT, there was no attenuation
150 of microinvasion with either the Δ*proABC/piaA* or Δ*fhs/piaA* strains, with a trend for greater
151 microinvasion (Fig 1C) with a higher microinvasive index (percentage of internalised bacteria /
152 associated bacteria; Supplemental Information Table 1).

153

154 ***S. pneumoniae* colonisation and microinvasion of primary human airway epithelium leads to**
155 **cellular reorganisation with retention of barrier function**

156 To further explore the impact of microinvasion on epithelial biology in a complex environment, we
157 cultured *S. pneumoniae* serotype 6B WT and the isogenic biosynthesis mutants with primary normal

158 human bronchial epithelial airway (NHBE-A) cells in air-liquid interface. We observed epithelial cell
159 association and microinvasion with all three strains (Fig2A, top). TEM demonstrated that intracellular
160 bacteria for all three strains were enclosed within vacuoles (Fig 2A, bottom). As seen previously with
161 several different pneumococcal strains (3), the 6B WT and the mutant strains co-localised with
162 Junctional Adhesion Molecule A (JAM-A, Supplemental Information Fig 1A, arrow), with no change
163 in overall JAM-A expression. However, using confocal microscopy and automated image analysis,
164 for cells infected with the 6B WT strain, we did observe an increase in the intensity of Zonula
165 Occludens 1 (ZO-1) staining at the junctional membrane (Supplementary Fig 1B), and a significant
166 increase in the intensity of β catenin staining for cells infected with either the Δ*proABC/piaA or*
167 Δ*fhs/piaA* strain (Fig 2B, 2C). These changes in junctional protein expression most likely occurred
168 as a result of cellular reorganisation, as de-novo protein production would have been insufficient
169 over the 6-hour experimental infection period. As measured by transepithelial electrical resistance,
170 barrier integrity was retained over the infection period, (Fig 2D).

171

172 When cultured at an air-liquid interface, NHBE cells differentiate into a typical pseudostratified
173 columnar ciliated epithelium, consisting of goblet, Clara, basal and ciliated cells (Fig 3A). Although
174 there was no predilection by *S. pneumoniae* for particular epithelial cell-types, pneumococci were
175 observed amongst cilia (acetylated tubulin positive cells, Fig 3B and Supplemental Information Fig
176 2) and co-localised with mucus (mucin5ac positive, Fig 3C, arrows). Strikingly, while the cellular
177 composition of the epithelial cultures exposed to the Δ*fhs/piaA* strain were comparable in
178 appearance to non-infected cells by SEM, exposure to the 6B WT and Δ*proABC/piaA* strains resulted
179 in an increased abundance in secreted mucus globules compared to non-infected cells (Fig 3A).
180 This appeared to be due to differential cellular secretion of preformed mucus rather than de-novo
181 production as these differences were not reflected in an increase in the expression of the gel-forming
182 glycoprotein Mucin5AC (Fig 3C and 3E, right graph). Following infection by the Δ*proABC/piaA* strain
183 we found a significant increase in expression of acetylated tubulin (Fig 3B and 3E, left graph), which
184 has been shown to be associated with increased microtubule conformation and elasticity, and occurs
185 by post-translational modification (22, 23). In contrast, following exposure to Δ*fhs/piaA* strain, we

186 saw an increased expression of the anti-inflammatory protein, uteroglobin (UG), which is a
187 multifunctional epithelial secreted protein with anti-inflammatory and anti-chemotactic properties,
188 and a marker for non-ciliated Clara cells (Fig 3D and 3F, left graph). These changes in UG
189 expression again most likely occurred as a result of cellular reorganisation, or secretion of pre-
190 formed protein, as de-novo protein production would have been insufficient to detect over the 6-hour
191 experimental infection period.

192

193 **Δ*proABC/piaA* and Δ*fhs/piaA* mutations of *S. pneumoniae* serotype 6B do not affect**
194 **microinvasion of Detroit 562 epithelial cells**

195 Detroit 562 epithelial nasopharyngeal cells enable the analysis of these host-pathogen interactions
196 under multiple conditions, which are not feasible with the primary cell lines. We have previously
197 shown that the pattern of Detroit 562 epithelial nasopharyngeal cell microinvasion, and subsequent
198 innate immune response to *S. pneumoniae* 6B infection *in vitro* is similar to that seen in the EPHC
199 *in vivo(3)*. We therefore then used Detroit 562 cells to further characterise colonisation by the WT,
200 Δ*proABC/piaA* and/or Δ*fhs/piaA* pneumococcal strains. We found that although all the strains formed
201 colonies on the epithelial surface (Fig 4A), the isogenic mutants associated less compared to 6B WT
202 (Fig 4B). Nonetheless, microinvasion was observed with all the strains (Fig 4C), with a significantly
203 elevated micro-invasive index for the Δ*proABC/piaA* and Δ*fhs/piaA* strains compared to WT (Fig 4D).
204 Differences in microinvasion were not due to differences in intracellular viability (Fig 4E) or replication
205 (Supplemental Information Fig 3A-F). All of the single and double biosynthesis genes mutants
206 (Δ*proABC*, Δ*fhs*, Δ*proABC/piaA*, Δ*fhs/piaA*) were impaired in their ability to transmigrate across the
207 epithelium (Fig 4F). Importantly, we show that a single Δp*iaA* mutation in the *S. pneumoniae* serotype
208 6B did not affect epithelial association, microinvasion and transmigration (Fig 4B, 4C, 4F).

209

210 Consistent with our previous findings for serotype 6B(3), Detroit 562 epithelial barrier function was
211 not compromised after three hours of infection; indeed, there was a tightening of the barrier
212 evidenced by reduced FITC dextran diffusion after pneumococcal exposure (Fig 4G). Pneumococcal

213 infection had no effect on Junctional Adhesion Molecule A (JAM-A), Zonula-Occludens 1 (ZO-1),
214 Claudin 1 or Claudin 4 expression (Supplemental Fig 4). However, we did observe a significant
215 increase in epithelial β catenin expression following incubation with the Δ*proABC/piaA* and Δ*fhs/piaA*
216 strains, compared to the WT (Fig 4H, 4I).
217

218 **Δ*fhs/piaA* but not the ΔproABC/piaA mutations attenuate the pro-inflammatory epithelial**
219 **innate response to pneumococcal colonisation and microinvasion**

220 We have previously shown that the Detroit 562 cell innate immune response to *S. pneumoniae* is
221 strain dependent (3). Having found that serotype 6B biosynthesis gene mutants that are attenuated
222 for disease retain their capacity for microinvasion, we have further assessed the link between
223 colonisation, microinvasion and epithelial cell innate immunity by RNAseq. Compared to non-
224 infected cells (Fig 5A), all strains upregulated 78 core epithelial genes related to cytokine signalling
225 in immune system, NLR signalling and GPCR ligand binding. 193 genes were upregulated by both
226 the 6B WT and Δ*proABC/piaA* strains, characterised by Rhodopsin-like receptors, GPCR ligand
227 binding, cytokine signalling in Immune system, signalling by interleukins and Toll Receptor cascades.
228 Infection with the Δ*fhs/piaA* strain resulted in a markedly different transcriptomic profile with modest
229 upregulation of 254 genes, characterised by antigen processing, proteasomal pathways, GTP
230 hydrolysis, and intracellular stress responses (Fig 5A). Overall, the epithelial genes that were most
231 upregulated following infection with 6B WT or Δ*proABC/piaA* strain were similar and contrasted to
232 the reduced gene expression profile seen with the Δ*fhs/piaA* strain despite high levels of cell invasion
233 (Fig 5B). Since both mutant strains contained the *piaA* mutation, this could not account for the
234 differences seen in these responses. Together, these data demonstrate that microinvasion, the
235 innate epithelial response and disease are not necessarily linked.

236

237 Transcription factors, cellular kinases and cytokines (Fig 5C, 5D) predicted to regulate the
238 differentially expressed genes, showed the greatest difference in profile following infection with
239 Δ*fhs/piaA* strain compared to infection with 6B WT and Δ*proABC/piaA* strains. Δ*fhs/piaA* was

240 predicted to show diminished NFκB and MAPK activation and was associated with a more intrinsic
241 and epithelial repair response that included TBK1, Raf1, JAK1 kinases and IL-1 and IL-33 cytokine
242 signalling.

243

244 **Enhanced epithelial caspase 8 activity following pneumococcal infection with the wild-type**
245 **and ∆proABC/piaA strains**

246 The NLRP3 inflammasome drives programmed epithelial cell death via caspase 1, caspase 3/7 and
247 caspase 8 activity (24). Caspase activity, primarily regulated post-translationally, enables a rapid
248 response to cellular stress and pathogen-mediated activation (25). In health, caspase regulation is
249 thought to be important for mucosal integrity (26). During bacterial pneumonia, caspase activation is
250 thought to have an important pro-inflammatory role, possibly triggered by pneumolysin (27, 28). We
251 have therefore explored whether the different patterns of microinvasion and epithelial reorganisation
252 seen with the WT 6B, and mutant strains are associated with differential caspase activation.

253

254 Compared to non-infected cells, infection with all strains led up to a 1.5-fold increase in epithelial
255 caspase activity 6-hour post infection (Fig 6A, dark grey bars). To test which caspases were
256 activated, we incubated infected cell cultures with either a caspase 1 inhibitor (YVAD-CHO), a
257 caspase 3/7 inhibitor (Z-VAD-FMK), or specifically measured caspase 8 activity. We found that the
258 increase was not due to caspase 1 activity (Fig 6B). Compared to non-infected cells, caspase 3/7
259 accounted for 3% and 15% of the caspase activity induced following infection with 6B WT and
260 ∆*fhs/piaA* strain respectively (Fig 6A). In contrast, ∆*proABC/piaA* strain did not induce caspase 3/7
261 activity. Significant caspase 8 activation was seen following infection with 6B WT and ∆*proABC/piaA*
262 strain, but not with the ∆*fhs/piaA* strain (Fig 6C).

263

264 Together, these data suggest differential caspase induction following infection with the different
265 strains, linking the proinflammatory profile of the 6B WT and the ∆*proABC/piaA* with caspase 8

266 activation, which we postulate may regulate pneumococcal survival and transmission during
267 colonisation in the nasopharynx.

268

269 **Deletion of the *proABC* and *fhs* genes have broad-ranging differential effects on the *S.***
270 ***pneumoniae* virulence gene expression and metabolic gene pathways when under stress**

271 We have previously found marked transcriptional differences between the WT and both mutants in
272 response to serum stress (used to represent the physiological stress found during human infection),
273 with an over three-fold increase in the number of genes upregulated by the mutant strains compared
274 to WT (17). Further analysis revealed that these genes include well-characterised pneumococcal
275 virulence factors such as *ply*, *nanA*, *psaA,* those regulating oxidative stress such as *SpxB*, *lctO* and
276 *adhE*, and genes involved in purine and carbohydrate metabolism (Supplemental Information Table
277 2). Phosphotransferase systems, amino nucleotide sugar, fructose and mannose and metabolic
278 pathways were the most significantly enriched pathways in the Δ*proABC* mutant under serum stress
279 (Table 1). In contrast, competence, purine, pyruvate, metabolic pathways, amino nucleotide sugar
280 pathways and secondary metabolites were the most significantly enriched pathways in the Δ*fhs*
281 mutant under stress (Table 1). Together these data suggest that deletion of the *proABC* and *fhs*
282 genes have widespread but differential effects on *S. pneumoniae* virulence and metabolism which
283 may explain then complex phenotypes seen following epithelial infection.

284

285 ***fhs* gene mutation in *S. pneumoniae* 6B is associated with increased pneumococcal hydrogen**
286 **peroxide secretion and decreased pneumolysin activity**

287

288 *S. pneumoniae* SpxB and LctO generate hydrogen peroxide (H_2O_2) which has been shown to
289 suppress ENaC-α transcription and inhibit the Na+–K+ pump, acting as an intracellular signal to
290 increase mitochondrial production of ROS (29, 30). We therefore postulated that differential
291 expression of pneumococcal H_2O_2 may modulate epithelial functional responses during

292 nasopharyngeal colonisation by *S. pneumoniae* and explain the differences in the epithelial innate
293 immune response to the 6B WT, Δ*proABC/piaA* and Δ*fhs/piaA* strains. To assess this, we measured
294 H_2O_2 concentration using a luminescence-based bioassay, normalising against bacterial CFU. After
295 three and six hours, we detected significantly higher levels of H_2O_2 in Δ*fhs/piaA* cultures compared
296 to 6B WT and Δ*proABC/piaA* strains (Fig 7A). Furthermore, this was not ameliorated by epithelial
297 cell contact (Fig. 7B).

298

299 The pore forming pneumococcal toxin pneumolysin can both activate and suppress the host innate
300 immune response and mediates the haemolytic activity characteristic of the pneumococcus (31-33).
301 H_2O_2 can increase the release of pneumolysin but paradoxically also negatively impairs its
302 haemolytic activity (34). Compatible with the latter and the higher production of H_2O_2 by the Δ*fhs*
303 */piaA* strain, despite having increased expression of *ply*, red blood cell lysis was reduced for Δ*fhs*
304 strains compared to 6B WT and Δ*proABC* (Fig. 7C).

305

306 Differential pneumococcal H_2O_2 release may therefore explain at least in part, the effects of the *S.*
307 *pneumoniae* serotype 6B WT and Δ*proABC /piaA* compared to the Δ*fhs /piaA* strain on the epithelial
308 response to colonisation and microinvasion. Importantly, in the 6-hour timeframe assessed, the
309 increased H_2O_2 release the Δ*fhs /piaA* strain was not associated with epithelial cellular toxicity or
310 loss of barrier function, but was associated with increased intracellular epithelial stress response, as
311 detected by RNAseq.

312

313

314 **DISCUSSION**

315 There is considerable variation in the propensity of different *S. pneumoniae* strains to colonise the
316 human host, cause invasive disease and transmit to others (1). During colonisation of the
317 nasopharyngeal niche, the pneumococcus was previously thought to be confined to the mucus layer

318 and the epithelial surface (1). However, using EHPC, we have previously reported that
319 pneumococcal microinvasion occurs in healthy volunteers (3), and we now show that even when
320 using isogenic serotype 6B pneumococcal biosynthesis pathway mutant strains that are attenuated
321 for systemic disease but not for carriage, this microinvasion is preserved (12). We found that
322 pneumococcal colonisation and microinvasion of primary human airway epithelium led to cellular
323 reorganisation and mucus production while retaining barrier function, although the pattern of this
324 reorganisation varied by strain. Furthermore, the pro-inflammatory innate response and caspase 8
325 activity associated with epithelial infection by *S. pneumoniae* serotype 6B were attenuated by the
326 Δ*fhs/piaA* but not by the Δ*proABC/piaA* mutation. Under stress conditions, along with presumably
327 compensatory changes in the expression of multiple metabolic pathways, the Δ*proABC* and Δ*fhs*
328 mutations resulted in the upregulation of several pneumococcal virulence factor genes (Graphical
329 Abstract Summary). Notably, the *fhs* gene mutation in *S. pneumoniae* serotype 6B was associated
330 with increased pneumococcal hydrogen peroxide secretion and decreased pneumolysin activity.
331 Together these findings suggest that despite being attenuated for disease, the metabolic changes
332 and the increased expression of pneumococcal virulence genes in response to stress may explain
333 the preservation of epithelial microinvasion by these mutants. However, although epithelial
334 microinvasion, cellular reorganisation, innate immune response, and the propensity to cause
335 invasive disease are strain dependent, these properties do not appear to be directly co-correlated.

336

337 The complexity of the interaction between *S. pneumoniae* and the mucosal epithelium was
338 highlighted through infection of our well-characterised primary epithelial cell model(35). The model
339 consisting of Clara cells (involved in secretory, xenobiotic metabolic, and progenitor cell functions),
340 goblet cells (mucus production), ciliated cells (responsible for mucus and small particle transport),
341 exhibited considerable epithelial cellular re-organisation involving β catenin, acetylated tubulin and
342 uteroglobin in response to pneumococcal infection. In a rabbit pneumococcal meningitis model,
343 increased acetylated tubulin and microtubule stabilisation was attributed to pneumolysin activity(23).
344 Previously, using a pneumolysin deficient mutant of *S. pneumoniae* serotype 4 (TIGR4), we have
345 shown that pneumolysin is a key driver of the epithelial inflammatory response to pneumococcal

346 infection (3). We therefore speculate that the differential expression of pneumolysin and H_2O_2 by the
347 WT and mutant strains may contribute to the differing patterns of epithelial reorganisation, and goblet
348 cell mucus release that we observed, and may impact on both clearance and transmission (1).

349

350 Epithelial infection with the 6B WT and Δ*proABC/piaA* strains induced innate inflammatory pathway
351 gene expression typical of pneumococcal infection (3), including cytokine/chemokines, interleukins,
352 Toll Like Receptor and NFκB signalling, alongside apoptotic transcripts such as FOXO3 and TP53.
353 We also identified epithelial genes upregulated only during WT infection, potentially related to a
354 greater disease-causing potential. These genes are involved in RNA degradation, O-linked
355 glycosylation, wnt signalling, DNA sensing, RIG-I pathways and signal transduction. In contrast, the
356 Δ*fhs/piaA* strain activated a pro-survival and adaptation profile, upregulating genes such as JUN,
357 SMARCA4, NFAT5, KLF6 and TCF4, which are involved in homeostatic signalling and chromatin
358 remodelling (36, 37), suggestive of a more tolerant response. Ultimately, these capsule-independent
359 differences in pneumococcal-epithelial interactions may shape the adaptive immune response to
360 pneumococcal colonisation (21, 38), which could then further influence the outcomes of both
361 colonisation and disease. How these findings translate to differences in the duration of
362 nasopharyngeal carriage, invasiveness, transmission or clearance remains to be fully determined.
363 However, during EHPC, Δ*fhs/piaA* infection was associated with increased density at day 6 post-
364 inoculation compared the other strains (20).

365

366 Importantly, while WT serotype 6B infection led to epithelial cell reorganisation (β catenin localisation
367 to the junctional membrane and mucus secretion), pneumococcal transmigration, a more pro-
368 inflammatory innate immune transcriptomic profile and increased caspase 8 activity, all indicative of
369 a robust cellular response to *S. pneumoniae*, the Δ*fhs/piaA* but not Δ*proABC/piaA* strains was
370 attenuated for many of these characteristics. This suggests that similar to the macrophage response
371 to *S. pneumoniae*, intracellular signalling by pneumococci is not the sole determinant of the epithelial
372 response to infection (32, 39). The *proABC* operon consists of three genes involved in proline

373 biosynthesis (ProABC)(40). *fhs* catalyses the synthesis of N10 formyl tetrahydrofolate, essential for
374 carbon metabolism and purine nucleotide biosynthesis in various bacterial species (16, 41),
375 especially under hypoxic conditions (41, 42). It is increasingly recognised that bacterial virulence and
376 metabolism are intimately linked (43). Whether the distinct epithelial innate immune response to
377 Δ*fhs/piaA* infection is due to diminished epithelial NFκB and MAPK activation (potentially linked to
378 extracellular receptor engagement), reduced caspase 8 activity mediated by enhanced
379 pneumococcal H_2O_2 release, decreased pneumolysin activity, or a compensatory metabolic
380 response to the stress remains to be determined.

381

382 *S. pneumoniae* is highly adapted to colonise the human host and transmit from person to person.
383 Invasive pneumococcal disease, particularly in its most severe forms, is a dead end for the bacteria.
384 Our observation that the induction of inflammation/ innate immunity is not necessarily linked to
385 disease potential supports our proposition that microinvasion during colonisation by the
386 pneumococcus may facilitate immune evasion. As is typical of 'professional' intracellular bacterial
387 species such as *Listeria* and *Salmonella*, the resulting host response might also promote
388 transmission (44, 45). Whether the less pro-inflammatory Δ*fhs/piaA* is less transmissible than the
389 more inflammatory WT remains to be determined but this could be further explored using EHPC
390 (46).

391

392 In conclusion, these data further support our proposed paradigm that epithelial microinvasion by *S.*
393 *pneumoniae* in healthy people is frequent and usually does not lead to disease. Our findings highlight
394 the broad-ranging effects of even single gene mutations in pneumococcal biosynthesis pathways,
395 which may partially explain the complexity of differences between seemingly closely related strains.
396 However, strain differences in subsequent epithelial cell microinvasion, cellular reorganisation and
397 inflammatory responses are likely driven by differential expression of a range of bacterial virulence
398 and metabolic pathways that are not necessarily co-correlated with disease-causing potential. As
399 suggested by our bacterial transcriptomic data, no single pneumococcal virulence factor or group of

400 factors fully explains the differences seen between the strains under stress. The complexity of these
401 bacterial-host cell interactions is modulated by mediators such as hydrogen peroxide and
402 pneumolysin, which can have both enhancing and inhibitory effects on the epithelial cell response to
403 infection in different contexts. *S. pneumoniae* in constantly evolving, with new variants emerging
404 both due to stochastic events and under ecological pressure from numerous factors including
405 vaccines and antibiotic exposure (47, 48) (49). Extensive phenotyping of emerging, genotypically
406 related pneumococcal strains offers the opportunity to more effectively unravel *S. pneumoniae*
407 pathogenesis and its adaptation to the nasopharyngeal niche.

408

409 **METHODS AND PROTOCOLS**

410

411 **Bacteria**

412 The *Streptococcus pneumoniae* serotype 6B (strain BHN 418(50)) was a kind gift from Prof. Birgitta
413 Henriques Normark (Karolinska Institute). Δ*proABC/piaA* and Δ*fhs/piaA* mutant strains were
414 generated using overlap extension PCR as described by Ramos-Sevillano *et al*(12). Stocks of
415 bacteria were stored at -80ºC when bacterial growth in Todd Hewitt Broth (THY) was 0.3 $O.D._{600nm}$.
416 Aliquots were defrosted, centrifuged at 8000g for eight minutes and resuspended in 1% Fetal Bovine
417 Serum (FBS, Gibco) in MEM media (Gibco) for infections. Approximately 10 bacteria were added for
418 every epithelial cell. Colony forming units (CFU) were counted by serial dilutions on horse blood agar
419 plates (EO Labs). Starting inoculums were not significantly different across strains for all assays.

420

421 **Bacterial RNA-seq sample collection, sequencing and reads**

422 Mutant pneumococcal strains (three biological replicates for each mutant) and 6B WT (three
423 biological replicates) were grown in THY to mid log phase and the pellets resuspended in THY and
424 undiluted human serum for 60mins. The culture was then pelleted, and RNA stored in RNA Protect
425 at -70ºC before extracting total RNA (17). Total RNA from each library was ribo-depleted and sent

426 for Illumina Next Seq Sequencing Pathogen Genomics Unit (PGU), UCL. The quality of raw FASTQ
427 reads was checked by FastQC v0.11.5, Babraham Bioinformatics, UK (51) and visualised using
428 multiQC v1.9 (52). Reads were trimmed using Trimmomatic 0.39 (53). Trimmed reads were also
429 checked by FastQC and multiQC. Trimmed reads were then mapped to KEGG annotated 6B
430 genome sequence (670-6B, Accession: CP002176.1) using bowtie2 with default settings(54).
431 Conversion into BAM files was performed using SAMtools (55). Mapped reads were visualized in
432 the Integrated Genome Browser (IGB) (56). FeatureCounts v2.0.0 was used to summarize read
433 counts for each annotated feature in the respective reference genomes in multimapping mode (-M)
434 (57).

435

436 **Differential gene expression analyses**

437 The generated count matrix was imported into R-studio (R v3.4.2) and normalization of counts and
438 differential gene expression analysis was performed by DESeq2 (58). DESeq2 normalized libraries
439 were regularized log transformed for visualizing heatmaps and clustering. Differential gene
440 expression was performed on raw counts. Fold change shrinkage was implemented with the apeglm
441 package within DESeq2. Genes with a log2 fold change > 1.5 and false discovery rate (FDR) of <
442 0.05 were categorized as differentially expressed. KEGG pathway enrichment and module analysis
443 were performed on differentially regulated genes using over representation analysis (ORA)
444 implemented by clusterProfiler (59).

445

446 **Experimental Human Pneumococcal Carriage Model (EHPC)**

447 A full explanation of experimental design and selection criteria has been previously described (3).
448 Following written informed consent, healthy non-smoking adults between the ages of 18 – 59 were
449 inoculated with 80,000 CFU/nostril live strains of *S. pneumoniae*. Mucosal cells from the inferior
450 turbinate using a plastic Rhino-probe™ (curettage, Arlington Scientific) were collected prior to
451 inoculation, and days 2 and 6 post-inoculation. Samples were processed for confocal microscopy
452 analysis. Nasal wash samples were collected for CFU count analysis. There were no adverse events.

453 Ethical approval was given by NHS Research and Ethics Committee (REC)/Liverpool School of
454 Tropical Medicine (LSTM) REC, reference number: 18/NW/0481 and Human Tissue Authority
455 licensing number 12548.
456
457 **Primary Human Epithelial Cells**
458 Normal Human Primary Bronchial/Tracheal Epithelial Cells (NHBE-A, ATCC® PCS-300-010™) were
459 plated at $6x10^3$ cells/cm^2 on a layer of sub-lethally γ-irradiated (60 Gy) mouse embryonic fibroblasts
460 3T3-J2 cells (kind donation from Howard Green, Harvard Medical School, Boston(60)) with
461 keratinocyte culture medium cFAD (3:1 DMEM (Gibco) to Ham F-12 Nut Mix (Gibco), 10% FBS
462 (HyClone, Sigma), 1% Penicillin-Streptomycin (100X, Sigma), 0.4 µg/mL Hydrocortisone
463 (Calbiochem, USA), 5 µg/ml Insulin (various), 10-10 Cholera Toxin (Sigma) and 2x10-9
464 Triodothyronine (Sigma)). Epithelial cells were stimulated with 10 ng/mL human epidermal growth
465 factor (hEGF, PeproTech, USA) on days 3 and 5. Cultures were grown at 37°C 6% CO_2 and sub-
466 confluent cultures were trypsinised with 0.25% Trypsin-EDTA (Sigma). For NHBE-A differentiation
467 in Air Liquid Interface (ALI) culture, cells were plated at a density of $6x10^4$/cm^2 on 1µm pore PET cell
468 culture inserts (12 wells, Greiner). The insert was supplemented with cFAD medium on the top and
469 bottom. After 48 hours, medium was removed from the top of the culture (exposure) and the culture
470 was fed with fresh PneumaCult™ differentiation Medium (Stemcell Technologies) from the bottom
471 of the well every 2 days for 3 weeks, until cell ciliation was observed. Antibiotics were removed from
472 the medium and cells washed 24 hours before infection experiments.
473
474 **Human Epithelial Cell Lines**
475 Human pharyngeal carcinoma Detroit 562 epithelial cells (ATCC_CCL-138) were grown in 10% FCS
476 in alpha MEM media (Gibco). For each set of experiments, cells were used within 5 passages. Cells
477 consistently tested PCR negative for mycoplasma (Cambridge Biosciences).
478
479 **Pneumococcal-epithelial cell co-culture**

480 For association and internalisation assays, confluent monolayers of Detroit 562 cells (typically day 7
481 - 8 post plating) cultured on 12 well plates (Corning), were exposed to *S. pneumoniae* (1 cell : 10
482 pneumococci) for three hours in 1% FCS alpha MEM (six-hour infection for HNBE-A cells in 1%
483 Pneumocult media without supplements) (3). Cells washed three times in $HBSS^{+/+}$ before incubation
484 in 1% saponin for 10 minutes at 37°C to lyse cells. Bacterial dilutions were plated on horse blood
485 agar for 16 hours and colony forming units counted. For internalisation quantification, 200µg/ml
486 gentamicin was added to the cells for one hour before incubation with saponin.
487
488 For transmigration assays, Detroit 562 cells were plated onto 3µm pore, PET Transwell Inserts
489 (ThermoFisher) typically for 10 days (3). Media was changed to 1% FCS (250µl apical chamber, 1ml
490 basal chamber) one hour prior to infection experiments. 1mg/ml FITC-dextran (Sigma Aldrich) was
491 added to the apical chamber of selected inserts for permeability assays. Transepithelial Electrical
492 Resistance (TEER) was measured before and after infection using an EVOM2 (World Precision
493 Instruments). Bacteria were added to the cells for three hours during of which 50µl of basal media
494 was repeatedly removed to measure bacterial load by counting CFU/well. Permeability was recorded
495 using a FLUOstar Omega (BMG Labtech) at 488nm.
496
497 **Confocal Microscopy**
498 Sample processing was performed as previously described(3). Briefly, mucosal cells from the EHPC
499 model were placed directly into 4% PFA and cytospun onto microscope slides. NHBE-A cells and
500 Detroit 562 cells cultured on transwell membranes were fixed in 4% PFA (Pierce, Methanol Free).
501 Cells were permeabilised with 0.2% Triton X-100 for 10 minutes, blocked for one hour in blocking
502 buffer (3% goat serum and 3% BSA in PBS (Sigma)) and incubated with pneumococcal antisera
503 Pool Q (raised against the polysaccharide capsule, SSI Diagnostica) for one hour. Wheat germ
504 agglutinin conjugated to Rhodamine (Vector Labs) was added along with goat-anti rabbit IgG
505 conjugated to Alexa Fluor 488 for 45 minutes in blocking buffer. Primary (used at 1:100) antibodies
506 used for epithelial cell proteins can be found in Supplemental Information Table 3. Secondary (used
507 at 1:500) antibodies were either goat anti-mouse or goat anti-rabbit – Alexa Fluor 555 or 546,
508 ThermoFisher. Of note, for epithelial protein antibodies raised in rabbit (Uteroglobin), no

509 pneumococcal staining was possible and therefore pneumococci were not visible on the images.
510 DAPI was added for 5 minutes and cells were mounted with Aqua PolyMount (VWR International)
511 and a coverslip on the microslide. Pneumococci were recorded by manual scanning of the whole
512 cytospin for the EHPC samples. More than three fields of view were recorded for each bacterial
513 strain for Detroit 562 cell infections, using inverted Zeiss LSM (either 700 or 880) confocal
514 microscopes. Images were processed with Zeiss LSM Image Browser. Z stacks were recorded at
515 1µm intervals at either 40x oil or 63x oil objectives. Automated image analysis was carried out using
516 Cellprofiler (61).

517

518 **Electron Microscopy**

519 Preparation of Detroit 562 cells and NHBE-A cells was identical, and previously described(3). Briefly,
520 cells cultured on transwells were fixed with 2% paraformaldehyde and 1.5% glutaraldehyde in 0.1 M
521 cacodylate buffer and post-fixed in 1% OsO4 / 1.5% K4Fe(CN)6 in 0.1 M cacodylate buffer pH7.3.
522 Samples were dehydrated in graded ethanol-water series and infiltrated with Agar 100 resin mix.
523 Ultra-thin sections were cut at 70-80 nm using a diamond knife on a Reichert ultracut microtome.
524 Sections were collected on 300 mesh copper grids and stained with lead citrate. For transmission
525 electron microscopy the samples were hardened at 60°C for 48 hours. The coverslip was removed,
526 and a representative area was selected. Ultra-thin sections were cut at 70-80 nm using a diamond
527 knife on a Reichert ultra-cut S microtome. Sections were collected on copper grids and stained with
528 lead citrate. Samples were viewed with a Joel 1010 transition electron microscope and the images
529 recorded using a Gatan Orius CCD camera.

530

531 **Pneumolysin activity**

532 Adapted from Kirkham et al(62). Briefly, final concentration of 2% horse blood (EO Labs) solution
533 was prepared in phenol free alpha MEM (Life Technologies) and 100 µl added to wells of a 96 U-
534 bottom plate (Corning). 100 µl of bacterial solutions (containing ~2.5×10^6 bacteria) were suspended
535 in phenol free alpha MEM were added to each 96 well. Saponin was used as a positive control for

536 lysis. Solutions were incubated for 30 minutes at 37°C before centrifugation at 1000g for one minute.
537 100 µl was transferred into a new 96 well plate and absorbance recorded at 540nm on a plate reader.
538

539 **Hydrogen Peroxide Assay**

540 Detroit 562 cells were cultured in white 96 well plates (Corning). NHBE-A cells were cultured in 12
541 well plates in Pneumocult media. Cells were incubated with H_2O_2 substrate and infected with strains
542 of *S. pneumoniae* for up to six hours according to manufacturers' instructions (ROS-Glo™ H_2O_2
543 Assay, Promega). ROS-Glo™ Detection solution was added to the cells and incubated for 20
544 minutes. For primary cells, supernatant was then transferred to a white 96 well plate. Luminescence
545 was read using a GloMax -Multi Detection System plate reader (Promega).
546

547 **Caspase assay**

548 Detroit 562 cells were cultured in white 96 well plates (Corning). NHBE-A cells were cultured in 12
549 well plates in Pneumocult media. Cells were infected with strains of *S. pneumoniae* for up to six
550 hours. Primary cell supernatant was transferred to a white 96 well plate. Samples were incubated
551 with Caspase-Glo® 1 Reagent, Caspase-Glo® 1 YVAD-CHO Reagent, Caspase-Glo® Z-VAD-FMK
552 Reagent or Caspase-Glo® 8 Reagent, for one hour and according to manufacturers' instructions
553 (Promega). Luminescence was read using a GloMax-Multi Detection System plate reader
554 (Promega).

555

556 RNA samples and sequencing (RNA-Seq)

557 RNA-Seq data was collected as previously described (3). Confluent monolayers of Detroit 562
558 epithelial cells were infected with S. pneumoniae strains for four hours before collection in RNALater.
559 RNA was extracted using a Qiagen RNAEasy micro kit and treated for DNA removal using a Qiagen
560 Turbo DNA-free kit. RNA quality was assessed and quantified using a BioAnalyser (Agilent 2100).
561 Samples were sequenced using Illumina Nextseq 500/550 High Output 75 cycle kit giving 15-20
562 million 41bp paired-end reads per sample (Pathogens Genomic Unit, UCL).

563

564 **Statistics**

565 Each condition within each experiment was performed in duplicate or triplicate, and each experiment
566 was performed independently more than three times, unless stated otherwise. Error bars represent
567 SEM, unless stated otherwise. GraphPad Prism Version 7 was used for parametric (t-tests or
568 ANOVA) or non-parametric (Mann-Whitney or Kruskal-Wallis tests) analysis, which was based on
569 the Shapiro-Wilk normality test. Ad hoc tests were performed using Tukey's (for parametric data) or
570 Dunn's (for non-parametric data) multiple comparisons test. P values less than 0.05 were considered
571 significant.

572

573 **Data and code availability**

574 Source data are provided as a Source Data file. RNAseq data from the Detroit 562 cell infections is
575 publicly accessible through Zenodo with Accession (DOI:10.5281/zenodo.7997789).

576

577 **ACKNOWLEDGEMENTS**

578 This study was funded by CMW from a Postdoctoral Innovation Award from UCL, a Pump-Priming
579 Award and Enhancement Award from the Human Infection Challenge Network for Vaccine
580 Development (HIC-VAC (funded by the GCRF Networks in Vaccines Research and Development)
581 which is co-funded by the MRC and BBSRC). This UK funded award is part of the EDCTP2
582 programme supported by the European Union. CMW and RSH are supported by the Medical
583 Research Council (grant MR/T016329/1). The authors would like to thank Prof. Peter Hermans
584 (Radboud University Medical Centre) for donating the 6B pneumococcal strain originally from Prof.
585 Birgitta Henriques-Normark (Karolinska Institute) and obtained directly from DF at LSTM. EHPC
586 sample collection was supported by the Medical Research Council (grant MR/M011569/1), Bill and
587 Melinda Gates Foundation (grant OPP1117728) awarded to DF and the National Institute for Health
588 Research (NIHR) Local Comprehensive Research Network. The authors also wish to thank the
589 EHPC Clinical Team at LSTM and all the volunteers. Confocal imaging facilities at LSTM were

590 funded by a Wellcome Trust Multi-User Equipment Grant (104936/Z/14/Z). Electron microscopy
591 processing and image capture was performed by Dr. Elizabeth Slavik-Smith in the Biosciences EM
592 facility at UCL. MC is supported by a Springboard to Independence grant (AirwayStasis) from the
593 French Government's Investissement d'Avenir program, the Laboratoire d'Excellence ''Integrative
594 Biology of Emerging Infectious Diseases" (ANR-10-LABX-62-IBEID) and the Chromatin and infection
595 unit headed by Melanie A. Hamon. RNA-Seq library preparation was undertaken at UCL through the
596 UCL/UCLH Biomedical Research Centre and MRC funded Pathogen Genomics Unit (PGU,
597 G0900950). All RNAseq data processing was completed by the PGU. MN is supported by the
598 Wellcome Trust and by NIHR Biomedical Research Centre Funding to University College Hospitals
599 NHS Foundation Trust and University College London. RR is supported by Marie Skłodowska-Curie
600 Individual Fellowships 896014. PB is supported by the European Research Council (ERC-Stg No.
601 639429), the Rosetrees Trust (M362-F1; M553), the CF Trust (SRC006;SRC020), the London
602 Advanced Therapies - Research England (C2N-AT.006), the MRC Confidence in Concept scheme
603 (Award: MC_PC_17180), the Innovate UK (Smart grant n.10005465), the Duchenne Parent Project
604 (DPP) and the NIHR GOSH BRC. MW is supported by a 223065 Wellcome Investigator Award to
605 Clare Jolly, UCL. ERS and JSB are supported by MRC grant R/N02687X/1 and Wellcome grant
606 221803/Z/20/Z. JSB is partially supported by the Department of Health's National Institute of Health
607 and Care Research Biomedical Research Centre funding to UCLH. RSH is a NIHR Senior
608 Investigator.
609

610 **AUTHOR CONTRIBUTIONS**: CMW conceived, funded, designed and conducted the study,
611 performed the experiments, acquired samples and processed data, and wrote the first draft of the
612 manuscript. GP analysed and interpreted the RNAseq data. MB analysed and interpreted the
613 bacterial transcriptomic data. RR cultured and differentiated primary epithelial cells. ERS generated
614 the 6B mutant strains and bacterial transcriptomic data. JR collected and processed EHPC samples.
615 JAGA processed the RNA-Seq data. MW ran the image analysis. MC provided technical advice. PB
616 and CJ provided investigator support. MN provided RNA-Seq analysis support. DF provided
617 investigator support and EHPC clinical samples. JSB generated the 6B mutant strains, interpreted

618 the data and revised the manuscript. RSH provided investigator support, designed and interpreted
619 the data, revised the manuscript. All authors commented on and approved the manuscript.

620

621 **COMPETING INTERESTS:** The authors declare no competing interests.

622

623 **REFERENCES**

624 1. Weiser JN, Ferreira DM, Paton JC. 2018. Streptococcus pneumoniae: transmission, colonization and
625 invasion. Nat Rev Microbiol 16:355-367.
626 2. O'Brien KL, Wolfson LJ, Watt JP, Henkle E, Deloria-Knoll M, McCall N, Lee E, Mulholland K, Levine OS,
627 Cherian T, Hib, Pneumococcal Global Burden of Disease Study T. 2009. Burden of disease caused by
628 Streptococcus pneumoniae in children younger than 5 years: global estimates. Lancet 374:893-902.
629 3. Weight CM, Venturini C, Pojar S, Jochems SP, Reine J, Nikolaou E, Solorzano C, Noursadeghi M, Brown
630 JS, Ferreira DM, Heyderman RS. 2019. Microinvasion by Streptococcus pneumoniae induces
631 epithelial innate immunity during colonisation at the human mucosal surface. Nat Commun 10:3060.
632 4. Zafar MA, Hamaguchi S, Zangari T, Cammer M, Weiser JN. 2017. Capsule Type and Amount Affect
633 Shedding and Transmission of Streptococcus pneumoniae. mBio 8.
634 5. Gladstone RA, Lo SW, Lees JA, Croucher NJ, van Tonder AJ, Corander J, Page AJ, Marttinen P, Bentley
635 LJ, Ochoa TJ, Ho PL, du Plessis M, Cornick JE, Kwambana-Adams B, Benisty R, Nzenze SA, Madhi SA,
636 Hawkins PA, Everett DB, Antonio M, Dagan R, Klugman KP, von Gottberg A, McGee L, Breiman RF,
637 Bentley SD, Global Pneumococcal Sequencing C. 2019. International genomic definition of
638 pneumococcal lineages, to contextualise disease, antibiotic resistance and vaccine impact.
639 EBioMedicine 43:338-346.
640 6. Amin-Chowdhury Z, Collins S, Sheppard C, Litt D, Fry NK, Andrews N, Ladhani SN. 2020.
641 Characteristics of Invasive Pneumococcal Disease Caused by Emerging Serotypes After the
642 Introduction of the 13-Valent Pneumococcal Conjugate Vaccine in England: A Prospective
643 Observational Cohort Study, 2014-2018. Clin Infect Dis 71:e235-e243.
644 7. Echlin H, Frank M, Rock C, Rosch JW. 2020. Role of the pyruvate metabolic network on carbohydrate
645 metabolism and virulence in Streptococcus pneumoniae. Mol Microbiol 114:536-552.
646 8. Hartel T, Eylert E, Schulz C, Petruschka L, Gierok P, Grubmuller S, Lalk M, Eisenreich W,
647 Hammerschmidt S. 2012. Characterization of central carbon metabolism of Streptococcus
648 pneumoniae by isotopologue profiling. J Biol Chem 287:4260-74.
649 9. Henriques-Normark B, Tuomanen EI. 2013. The pneumococcus: epidemiology, microbiology, and
650 pathogenesis. Cold Spring Harb Perspect Med 3.
651 10. Kohler S, Voss F, Gomez Mejia A, Brown JS, Hammerschmidt S. 2016. Pneumococcal lipoproteins
652 involved in bacterial fitness, virulence, and immune evasion. FEBS Lett 590:3820-3839.
653 11. van Opijnen T, Camilli A. 2012. A fine scale phenotype-genotype virulence map of a bacterial
654 pathogen. Genome Res 22:2541-51.
655 12. Ramos-Sevillano E, Ercoli G, Felgner P, Ramiro de Assis R, Nakajima R, Goldblatt D, Heyderman RS,
656 Gordon SB, Ferreira DM, Brown JS. 2020. Preclinical Development of Virulence Attenuated
657 Streptococcus pneumoniae Strains Able to Enhance Protective Immunity Against Pneumococcal
658 Infection. Am J Respir Crit Care Med doi:10.1164/rccm.202011-4161LE.
659 13. Ogunniyi AD, Mahdi LK, Trappetti C, Verhoeven N, Mermans D, Van der Hoek MB, Plumptre CD, Paton
660 JC. 2012. Identification of genes that contribute to the pathogenesis of invasive pneumococcal
661 disease by in vivo transcriptomic analysis. Infect Immun 80:3268-78.

662 14. Mahdi LK, Wang H, Van der Hoek MB, Paton JC, Ogunniyi AD. 2012. Identification of a novel
663 pneumococcal vaccine antigen preferentially expressed during meningitis in mice. J Clin Invest
664 122:2208-20.
665 15. Brill J, Hoffmann T, Bleisteiner M, Bremer E. 2011. Osmotically controlled synthesis of the compatible
666 solute proline is critical for cellular defense of Bacillus subtilis against high osmolarity. J Bacteriol
667 193:5335-46.
668 16. Crowley PJ, Gutierrez JA, Hillman JD, Bleiweis AS. 1997. Genetic and physiologic analysis of a formyl-
669 tetrahydrofolate synthetase mutant of Streptococcus mutans. J Bacteriol 179:1563-72.
670 17. Ramos-Sevillano E. EG, Guerra-Assunção J.F., Betts M., Partridge F., Fernandes V.E., Wall E., Gordon
671 S.B., Ferreira D.M., Heyderman R.S., Brown J.S. 2023. Essential role of proline synthesis and the one-
672 carbon metabolism pathways for systemic virulence of Streptococcus pneumoniae. Biorxiv
673 doi:https://doi.org/10.1101/2023.08.03.550501.
674 18. Brown JS, Gilliland SM, Holden DW. 2001. A Streptococcus pneumoniae pathogenicity island
675 encoding an ABC transporter involved in iron uptake and virulence. Mol Microbiol 40:572-85.
676 19. Hill H, Mitsi E, Nikolaou E, Blizard A, Pojar S, Howard A, Hyder-Wright A, Devin J, Reine J, Robinson R,
677 Solorzano C, Jochems SP, Kenny-Nyazika T, Ramos-Sevillano E, Weight CM, Myerscough C,
678 McLenaghan D, Morton B, Gibbons E, Farrar M, Randles V, Burhan H, Chen T, Shandling AD, Campo
679 JJ, Heyderman RS, Gordon SB, Brown JS, Collins AM, Ferreira DM. 2023. A Randomised Controlled
680 Trial of Nasal Immunisation with Live Virulence Attenuated Streptococcus pneumoniae Strains Using
681 Human Infection Challenge. Am J Respir Crit Care Med doi:10.1164/rccm.202302-0222OC.
682 20. Hill H ME, Nikolaou E, Blizard A, Pojar S, Howard A, Hyder-Wright A, Devin J, Reiné J, Robinson R,
683 Solórzano C, Jochems S, Kenny-Nyazika T, Ramos-Sevillano E, Weight CM, Myerscough C, McLennan
684 D, MortonB , Gibbons E, Farrar M, Randles V, Burhan H, Chen T, Shandling AD, Campo JJ, Heyderman
685 RS, Gordon SB, Brown JS, Collins AM, Ferreira DM. 2023. A Randomised Controlled Trial of Nasal
686 Immunisation with Live Virulence Attenuated Streptococcus pneumoniae Strains using Human
687 Infection Challenge. Medrxiv doi:https://doi.org/10.1101/2023.04.14.23288224.
688 21. Ferreira DM, Neill DR, Bangert M, Gritzfeld JF, Green N, Wright AK, Pennington SH, Bricio-Moreno L,
689 Moreno AT, Miyaji EN, Wright AD, Collins AM, Goldblatt D, Kadioglu A, Gordon SB. 2013. Controlled
690 human infection and rechallenge with Streptococcus pneumoniae reveals the protective efficacy of
691 carriage in healthy adults. Am J Respir Crit Care Med 187:855-64.
692 22. Eshun-Wilson L, Zhang R, Portran D, Nachury MV, Toso DB, Lohr T, Vendruscolo M, Bonomi M, Fraser
693 JS, Nogales E. 2019. Effects of alpha-tubulin acetylation on microtubule structure and stability. Proc
694 Natl Acad Sci U S A 116:10366-10371.
695 23. Iliev AI, Djannatian JR, Opazo F, Gerber J, Nau R, Mitchell TJ, Wouters FS. 2009. Rapid microtubule
696 bundling and stabilization by the Streptococcus pneumoniae neurotoxin pneumolysin in a
697 cholesterol-dependent, non-lytic and Src-kinase dependent manner inhibits intracellular trafficking.
698 Mol Microbiol 71:461-77.
699 24. Surabhi S, Jachmann LH, Shumba P, Burchhardt G, Hammerschmidt S, Siemens N. 2022. Hydrogen
700 Peroxide Is Crucial for NLRP3 Inflammasome-Mediated IL-1beta Production and Cell Death in
701 Pneumococcal Infections of Bronchial Epithelial Cells. J Innate Immun 14:192-206.
702 25. Maekawa T, Kashkar H, Coll NS. 2023. Dying in self-defence: a comparative overview of immunogenic
703 cell death signalling in animals and plants. Cell Death Differ 30:258-268.
704 26. Gunther C, Buchen B, He GW, Hornef M, Torow N, Neumann H, Wittkopf N, Martini E, Basic M, Bleich
705 A, Watson AJ, Neurath MF, Becker C. 2015. Caspase-8 controls the gut response to microbial
706 challenges by Tnf-alpha-dependent and independent pathways. Gut 64:601-10.
707 27. Gonzalez-Juarbe N, Bradley KM, Shenoy AT, Gilley RP, Reyes LF, Hinojosa CA, Restrepo MI, Dube PH,
708 Bergman MA, Orihuela CJ. 2017. Pore-forming toxin-mediated ion dysregulation leads to death
709 receptor-independent necroptosis of lung epithelial cells during bacterial pneumonia. Cell Death
710 Differ 24:917-928.
711 28. Gonzalez-Juarbe N, Bradley KM, Riegler AN, Reyes LF, Brissac T, Park SS, Restrepo MI, Orihuela CJ.
712 2018. Bacterial Pore-Forming Toxins Promote the Activation of Caspases in Parallel to Necroptosis to
713 Enhance Alarmin Release and Inflammation During Pneumonia. Sci Rep 8:5846.

714 29. Erttmann SF, Gekara NO. 2019. Hydrogen peroxide release by bacteria suppresses inflammasome-
715 dependent innate immunity. Nat Commun 10:3493.
716 30. Alibayov B, Scasny A, Khan F, Creel A, Smith P, Vidal AGJ, Fitisemanu FM, Padilla-Benavides T, Weiser
717 JN, Vidal JE. 2022. Oxidative Reactions Catalyzed by Hydrogen Peroxide Produced by Streptococcus
718 pneumoniae and Other Streptococci Cause the Release and Degradation of Heme from Hemoglobin.
719 Infect Immun 90:e0047122.
720 31. Zafar MA, Wang Y, Hamaguchi S, Weiser JN. 2017. Host-to-Host Transmission of Streptococcus
721 pneumoniae Is Driven by Its Inflammatory Toxin, Pneumolysin. Cell Host Microbe 21:73-83.
722 32. Periselneris J, Turner CT, Ercoli G, Szylar G, Weight CM, Thurston T, Whelan M, Tomlinson G,
723 Noursadeghi M, Brown J. 2022. Pneumolysin suppresses the initial macrophage pro-inflammatory
724 response to Streptococcus pneumoniae. Immunology 167:413-427.
725 33. Terra VS, Plumptre CD, Wall EC, Brown JS, Wren BW. 2020. Construction of a pneumolysin deficient
726 mutant in streptococcus pneumoniae serotype 1 strain 519/43 and phenotypic characterisation.
727 Microb Pathog 141:103999.
728 34. Bazant J, Ott B, Hudel M, Hain T, Lucas R, Mraheil MA. 2023. Impact of Endogenous Pneumococcal
729 Hydrogen Peroxide on the Activity and Release of Pneumolysin. Toxins (Basel) 15.
730 35. Travaglini KJ, Nabhan AN, Penland L, Sinha R, Gillich A, Sit RV, Chang S, Conley SD, Mori Y, Seita J,
731 Berry GJ, Shrager JB, Metzger RJ, Kuo CS, Neff N, Weissman IL, Quake SR, Krasnow MA. 2020. A
732 molecular cell atlas of the human lung from single-cell RNA sequencing. Nature 587:619-625.
733 36. Herta T, Bhattacharyya A, Bollensdorf C, Kabus C, Garcia P, Suttorp N, Hippenstiel S, Zahlten J. 2018.
734 DNA-release by Streptococcus pneumoniae autolysin LytA induced Krueppel-like factor 4 expression
735 in macrophages. Sci Rep 8:5723.
736 37. Barutcu AR, Lajoie BR, Fritz AJ, McCord RP, Nickerson JA, van Wijnen AJ, Lian JB, Stein JL, Dekker J,
737 Stein GS, Imbalzano AN. 2016. SMARCA4 regulates gene expression and higher-order chromatin
738 structure in proliferating mammary epithelial cells. Genome Res 26:1188-201.
739 38. Wilson R, Cohen JM, Jose RJ, de Vogel C, Baxendale H, Brown JS. 2015. Protection against
740 Streptococcus pneumoniae lung infection after nasopharyngeal colonization requires both humoral
741 and cellular immune responses. Mucosal Immunol 8:627-39.
742 39. Periselneris J, Ercoli G, Pollard T, Chimalapati S, Camberlein E, Szylar G, Hyams C, Tomlinson G,
743 Petersen FC, Floto RA, Noursadeghi M, Brown JS. 2019. Relative Contributions of Extracellular and
744 Internalized Bacteria to Early Macrophage Proinflammatory Responses to Streptococcus
745 pneumoniae. mBio 10.
746 40. Belitsky BR, Brill J, Bremer E, Sonenshein AL. 2001. Multiple genes for the last step of proline
747 biosynthesis in Bacillus subtilis. J Bacteriol 183:4389-92.
748 41. Sah S, Aluri S, Rex K, Varshney U. 2015. One-carbon metabolic pathway rewiring in Escherichia coli
749 reveals an evolutionary advantage of 10-formyltetrahydrofolate synthetase (Fhs) in survival under
750 hypoxia. J Bacteriol 197:717-26.
751 42. Aluri S, Rex K, Varshney U. 2015. Simultaneous presence of fhs and purT genes is disadvantageous
752 for the fitness of Escherichia coli growth. FEMS Microbiol Lett 362.
753 43. Obolski U, Swarthout TD, Kalizang'oma A, Mwalukomo TS, Chan JM, Weight CM, Brown C, Cave R,
754 Cornick J, Kamng'ona AW, Msefula J, Ercoli G, Brown JS, Lourenco J, Maiden MC, French N, Gupta S,
755 Heyderman RS. 2023. The metabolic, virulence and antimicrobial resistance profiles of colonising
756 Streptococcus pneumoniae shift after PCV13 introduction in urban Malawi. Nat Commun 14:7477.
757 44. Galan JE. 2021. Salmonella Typhimurium and inflammation: a pathogen-centric affair. Nat Rev
758 Microbiol 19:716-725.
759 45. Li G, Wang G, Li M, Li L, Liu H, Sun M, Wen Z. 2020. Morin inhibits Listeria monocytogenes virulence
760 in vivo and in vitro by targeting listeriolysin O and inflammation. BMC Microbiol 20:112.
761 46. Connor V, German E, Pojar S, Mitsi E, Hales C, Nikolaou E, Hyder-Wright A, Adler H, Zaidi S, Hill H,
762 Jochems SP, Burhan H, French N, Tobery T, Rylance J, Ferreira DM. 2018. Hands are vehicles for
763 transmission of Streptococcus pneumoniae in novel controlled human infection study. Eur Respir J
764 52.
765 47. Lourenco J, Daon Y, Gori A, Obolski U. 2021. Pneumococcal Competition Modulates Antibiotic
766 Resistance in the Pre-Vaccination Era: A Modelling Study. Vaccines (Basel) 9.

767 48. Watkins ER, Kalizang'Oma A, Gori A, Gupta S, Heyderman RS. 2022. Factors affecting antimicrobial
768 resistance in Streptococcus pneumoniae following vaccination introduction. Trends Microbiol
769 30:1135-1145.
770 49. Chaguza C, Senghore M, Bojang E, Gladstone RA, Lo SW, Tientcheu PE, Bancroft RE, Worwui A, Foster-
771 Nyarko E, Ceesay F, Okoi C, McGee L, Klugman KP, Breiman RF, Barer MR, Adegbola RA, Antonio M,
772 Bentley SD, Kwambana-Adams BA. 2020. Within-host microevolution of Streptococcus pneumoniae
773 is rapid and adaptive during natural colonisation. Nat Commun 11:3442.
774 50. Browall S, Norman M, Tangrot J, Galanis I, Sjostrom K, Dagerhamn J, Hellberg C, Pathak A, Spadafina
775 T, Sandgren A, Battig P, Franzen O, Andersson B, Ortqvist A, Normark S, Henriques-Normark B. 2014.
776 Intraclonal variations among Streptococcus pneumoniae isolates influence the likelihood of invasive
777 disease in children. J Infect Dis 209:377-88.
778 51. S. A. 2010. FastQC: a quality control tool for high throughput sequence data.
779 52. Ewels P, Magnusson M, Lundin S, Kaller M. 2016. MultiQC: summarize analysis results for multiple
780 tools and samples in a single report. Bioinformatics 32:3047-8.
781 53. Bolger AM, Lohse M, Usadel B. 2014. Trimmomatic: a flexible trimmer for Illumina sequence data.
782 Bioinformatics 30:2114-20.
783 54. Langmead B, Salzberg SL. 2012. Fast gapped-read alignment with Bowtie 2. Nat Methods 9:357-9.
784 55. Li H, Handsaker B, Wysoker A, Fennell T, Ruan J, Homer N, Marth G, Abecasis G, Durbin R, Genome
785 Project Data Processing S. 2009. The Sequence Alignment/Map format and SAMtools. Bioinformatics
786 25:2078-9.
787 56. Nicol JW, Helt GA, Blanchard SG, Jr., Raja A, Loraine AE. 2009. The Integrated Genome Browser: free
788 software for distribution and exploration of genome-scale datasets. Bioinformatics 25:2730-1.
789 57. Liao Y, Smyth GK, Shi W. 2014. featureCounts: an efficient general purpose program for assigning
790 sequence reads to genomic features. Bioinformatics 30:923-30.
791 58. Love MI, Huber W, Anders S. 2014. Moderated estimation of fold change and dispersion for RNA-seq
792 data with DESeq2. Genome Biol 15:550.
793 59. Yu G, Wang LG, Han Y, He QY. 2012. clusterProfiler: an R package for comparing biological themes
794 among gene clusters. OMICS 16:284-7.
795 60. Rheinwald JG, Green H. 1975. Serial cultivation of strains of human epidermal keratinocytes: the
796 formation of keratinizing colonies from single cells. Cell 6:331-43.
797 61. Carpenter AE, Jones TR, Lamprecht MR, Clarke C, Kang IH, Friman O, Guertin DA, Chang JH, Lindquist
798 RA, Moffat J, Golland P, Sabatini DM. 2006. CellProfiler: image analysis software for identifying and
799 quantifying cell phenotypes. Genome Biol 7:R100.
800 62. Kirkham LA, Kerr AR, Douce GR, Paterson GK, Dilts DA, Liu DF, Mitchell TJ. 2006. Construction and
801 immunological characterization of a novel nontoxic protective pneumolysin mutant for use in future
802 pneumococcal vaccines. Infect Immun 74:586-93.

803

804

805 **FIGURE LEGENDS**

806 **Table 1. Differentially expressed pathways from single isogenic mutants in human**
807 **serum compared to WT.** 55 genes were selected within competence pathways, amino acid
808 metabolism, virulence factors, oxidative stress pathways and other known genes important
809 for colonisation, for assessment of changes in gene expression following serum stress. *q*-

810 *value* measures the proportion of false positives incurred (the false discovery rate) when
811 that particular test is significant.

812

813 **Fig 1. Pneumococcal – epithelial interactions in the EHPC model**. (A) Schematic showing that
814 during colonisation, pneumococci adhere to the epithelial cell surface (association), internalise inside
815 epithelial cells (microinvasion). Mucus – lime; pneumococci – purple; intracellular vacuole – dark
816 green; epithelial cells – yellow; nucleus – brown; cell junctions – pink. (B) Representative microscopy
817 images showing 6B association to the epithelium and microinvasion by the Δ*proABC/piaA* or
818 Δ*fhs/piaA* mutants. Surface carbohydrates (red), nuclei (DAPI, blue), pneumococci (green). (C)
819 Table summarising the percentage of bacteria that were found by microscopy, on the surface
820 (association) or inside (microinvasion) cells in the EHPC model. Mucosal curettage samples were
821 collected at day 6 post-pneumococcal challenge. Number of volunteers (n) in each group is indicated
822 in brackets, along with the total numbers of pneumococci (Spn) counted.

823

824 **Fig 2. Impact of pneumococcal infection on NHBE-A cell junctional protein expression and**
825 **barrier integrity.** NHBE-A Cells were cultured at ALI and infected with pneumococcal strains for
826 6hrs. (A) Top: Representative confocal microscopy images from 4 independent experiments with
827 replicates, showing pneumococcal (green) association with the epithelium (red, surface
828 carbohydrates; nuclei blue) at 6hr post infection. Bottom: Representative transmission electron
829 microscopy images from 2 independent experiments, showing pneumococcal microinvasion
830 examples of each strain (arrows), enclosed within a vacuole after 4hr infection. (B) Representative
831 confocal microscopy images from 4 independent experiments with replicates, showing
832 pneumococcal (green) interactions with junctional proteins (red) of β catenin. Colocalization of red
833 and green appears yellow. Nuclei (blue). (C) Integrated intensity of β catenin in pneumococcal
834 negative (not pneumococcal associated) or positive (pneumococcal associated) cells. Non infected
835 v pneumococcal negative cells **** p <0.0001 (NI v Δ*proABC/piaA*), ** p = 0.0026 (NI v Δ*fhs/piaA*);
836 non-infected v pneumococcal positive cells; **** p <0.0001 (NI v Δ*proABC/piaA* and NI v Δ*fhs/piaA*);

837 Kruskal-Wallis, n = 4 independent experiments. (D) Transepithelial electrical resistance (TEER) was
838 recorded pre- and post- 6hr infection to assess barrier integrity. N = 3 independent experiments with
839 replicates. Average TEER pre-infection was 466Ω.cm^2 (430-484 Ω.cm^2, p = 0.1458 ANOVA) and
840 average TEER post-infection was 545Ω.cm^2 (527-567 Ω.cm^2. p = 0.04744 ANOVA). Change in
841 TEER comparing non-infected cells to infected cells p = 0.6592, Kruskal-Wallis. Error bars represent
842 SEM.

843

844 **Fig 3. Pneumococcal – epithelial interactions with primary human epithelial cells.** Cells were
845 cultured at ALI and infected with pneumococcal strains for 6hrs. (A) Representative scanning
846 electron microscopy images from 2 independent experiments, showing the surface of the epithelium.
847 Representative examples of differentiated epithelia (basal cells, Clara cells, goblet cells, ciliated
848 cells) are shown in yellow text. Colonising pneumococci are highlighted by arrows. Representative
849 confocal microscopy images from 4 independent experiments with replicates for (B) Ciliated cells
850 (acetylated tubulin, red), (C) Goblet cells (mucin5ac, red, (arrows indicate co-localisation of
851 mucin5ac with pneumococci)), (D) Clara cells (uteroglobin, red) after 6hr infection. Pneumococci
852 (green), nuclei (DAPI, blue), colocalization of red and green appears as yellow. (E) Integrated
853 intensity of acetylated tubulin and Muc5ac in pneumococcal negative or positive cells from two or
854 more images. Acetylated tubulin, neg p = 0.2677, pos p = 0.017; Mucin5ac, neg p = 0.6852, pos p =
855 0.8510, ANOVA. N = 3 or 4 independent experiments. (F) Integrated intensity of uteroglobin
856 normalised to non-infected cells (left, p = 0.0115 non-infected v infected, Kruskal-Wallis) and
857 percentage of Clara positive cells following infection (right, p = 0.0003 non-infected v strains, p =
858 0.0036 6B v mutant strains, Kruskal-Wallis). N = 3 independent experiments.

859

860 **Fig 4**. **Strain association, microinvasion and transmigration of Detroit 562 cells.** Cells were
861 infected with *S. pneumoniae* for three hours and CFU counts recorded. (A) Representative confocal
862 microscopy images from 6 independent experiments with replicates, showing pneumococcal (green)
863 interactions with surface carbohydrates (red). (B) Association of pneumococcal strains to epithelial
864 cells. p = 0.0009 (Kruskal-Wallis), n = 6 with replicates. (C) Internalisation of strains into cells,

865 following a gentamicin protection assay. p = 0.0219 (Kruskal-Wallis) N = 6 with replicates. (D)
866 Microinvasive index is defined as the percentage of internalised bacteria over all associated bacteria.
867 p = 0.071 (Kruskal-Wallis) N = 6 with replicates. (E) Pneumococcal viability inside epithelial cells
868 following a gentamicin protection assay. n = 3 or 4 independent experiments with replicates. Counts
869 were normalised to microinvasion counts for each strain after 3 hours infection and compared to 6B
870 WT; +1hr p = 0.6517, +2hr p = 0.1377, +3hr p = 0.1183 (ANOVA). (F) Transmigration of
871 pneumococcal strains across confluent monolayers on transwell inserts. CFUs were recorded from
872 the basal chamber. N = 6 independent experiments with replicates. p < 0.001 (Kruskal-Wallis). (G)
873 Epithelial cell permeability was assessed via leak to 4kDa FITC-Dextran into the basal chamber. N
874 = 4 with replicates. p <0.0001 compared to non-infected cells, and p = 0.0689 between 6B WT and
875 mutant strains (Kruskal-Wallis). (H) Representative confocal microscopy images from 6 independent
876 experiments with replicates, showing pneumococcal (green) interactions with β catenin (red).
877 Nuclear DAPI stain (blue). (I) Image quantification of integrated intensity of β catenin normalised to
878 non-infected cells, following infection with the different strains. N = 5 independent experiments. Non
879 infected v pneumococcal negative cells **** p <0.0001 (NI v Δ*fhs/piaA*); non-infected v
880 pneumococcal positive cells; **** p <0.0001 (NI v 6B), * p = 0.0183 (NI v Δ*proABC/piaA*), * p = 0.0149
881 (NI v Δ*fhs/piaA*); Kruskal-Wallis.

882

883 **Fig 5. Detroit 562 cell transcriptomic responses to pneumococcal strains.** Epithelial cells were
884 infected for four hours with pneumococcal strains and RNA extracted and processed for RNAseq.
885 6B n = 11, PP n = 17, FP n = 14, non-infected n = 12, from 6 independent experiments. (A) All
886 significantly log2 fold change upregulated genes according to strain compared to non-infected cells.
887 Significance was defined as DEGs with a log2 fold change (logFC) of > 1.5 and false discovery rate
888 (FDR) of < 0.05. (B) Comparison of the top 20 most upregulated genes for each strain, compared to
889 non-infected cells. Upstream regulator analysis for (C) transcription factors and (D) kinases.

890

891 **Fig 6. Effects of pneumococcal infection on caspase activity in Detroit 562 cells.** Caspase
892 activity was assessed by luminescence, following infection with pneumococcal strains for 6 hours.

893 (A) Caspase 3/7 activity was determined following incubation with the specific inhibitor Z-VAD-FMK.
894 N = 4 with replicates. In comparison to non-infected cells, caspase 3/7 $p = 0.0022$; caspase 3/7 + Z-
895 VAD-FMK inhibitor $p = 0.0005$. In comparison to 6B WT, caspase 3/7 $p = 0.0215$; caspase 3/7 + Z-
896 VAD-FMK inhibitor $p = 0.0012$ (Kruskal-Wallis). (B) Caspase 1 activity was determined following
897 incubation with the specific inhibitor YVAD-CHO. Negative signals indicate caspase activity other
898 than caspase 1. N = 6 with replicates. In comparison to non-infected cells, $p = 0.39$; caspase+YVAD-
899 CHO inhibitor $p = 0.3604$ and, in comparison to 6B WT, $p = 0.6226$; caspase+YVAD-CHO inhibitor
900 $p = 0.5386$ (Kruskal-Wallis). (C) Caspase 8 activity was assessed following infection with
901 pneumococcal strains. N = 3 with replicates. In comparison to non-infected cells, $p = 0.0015$
902 (ANOVA) and, in comparison to 6B WT, $p = 0.0172$ (ANOVA).

903

904 **Fig 7. Hydrogen peroxide secretion and pneumolysin activity from pneumococcal strains in**
905 **the absence and presence of Detroit 562 cells.** A) Fold change of hydrogen peroxide production
906 from the mutants compared to WT, normalised to the CFU counts. 3hr $p = 0.0087$ (ANOVA), 6hr p
907 $= 0.0209$ (Kruskal-Wallis). B) Fold change of hydrogen peroxide production from the mutants
908 compared to WT, normalised to the CFU counts, following infection of Detroit 562 cells. Media was
909 replaced after 1hr infection and cells incubated for a further 5hrs. N = 3 independent experiments
910 with replicates. Compared to 6B WT, $p = 0.0034$ (ANOVA). C) Pneumolysin activity was assessed
911 using a red blood cell lysis assay. Strains were incubated with red blood cells for 30 minutes and
912 absorbance measured. N = 4 experiments with replicates. Pneumococcal strain haemolytic activity
913 is calculated in comparison to 100% lysis by 0.0625% saponin. $p < 0.0001$ compared to 6B WT
914 (ANOVA).

Table 1. Differentially expressed pathways from single isogenic mutants in human serum compared to WT.

Pathway	GeneRatio	P-adjust	qvalue
Δ*fhs* vs. WT			
Fatty acid metabolism/biosynthesis	10/57	1.08E-09	6.49E-10
Biosynthesis of secondary metabolites	26/57	2.09E-04	1.26E-04
Purine metabolism	10/57	1.34E-03	8.06E-04
Quorum sensing	11/57	3.20E-03	1.92E-03
Pantothenate and CoA biosynthesis	5/57	3.59E-03	2.16E-03
beta-Lactam resistance	5/57	7.59E-03	4.57E-03
Propanoate metabolism	4/57	1.51E-02	9.09E-03
2-Oxocarboxylic acid metabolism	4/57	1.51E-02	9.09E-03
Metabolic pathways	40/57	1.94E-02	1.16E-02
Amino sugar and nucleotide sugar metabolism	7/57	4.22E-02	2.54E-02
Pyruvate metabolism	5/57	4.31E-02	2.59E-02
Δ*proABC* vs. WT			
Fatty acid metabolism/biosynthesis	10/71	1.17E-08	8.94E-09
Galactose metabolism	12/71	1.25E-04	2.47E-08
Phosphotransferase system (PTS)	13/71	2.54E-03	1.93E-03
Amino sugar and nucleotide sugar metabolism	9/71	2.89E-02	2.20E-02

Figure 1. Pneumococcal – epithelial interactions in the EHPC model

A

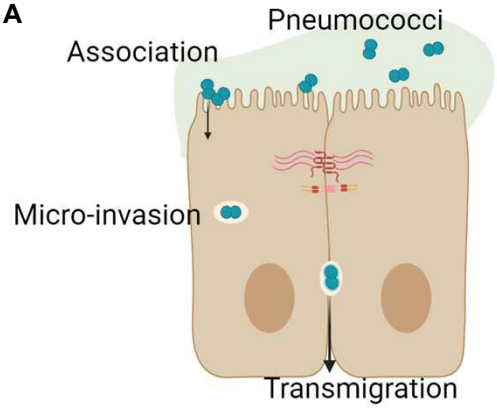

B

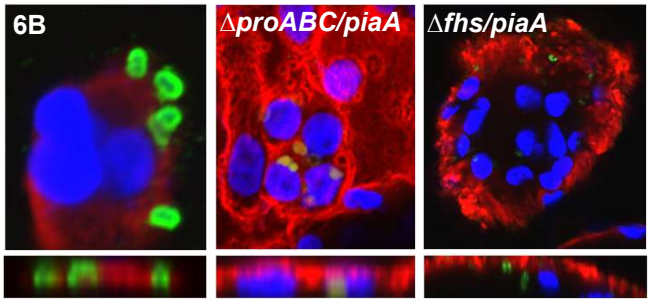

C

	Day 6 post-challenge	
	Association (%)	**Micro-invasion (%)**
6B	87.8 (n11, 43spn)	12.2 (n11, 6spn)
Δ*proABC/piaA*	59.3 (n11, 16spn)	40.7 (n11, 11spn)
Δ*fhs/piaA*	48.7 (n5, 57spn)	51.3 (n5, 60spn)

Figure 2. Impact of pneumococcal infection on NHBE-A cell junctional protein expression and barrier integrity.

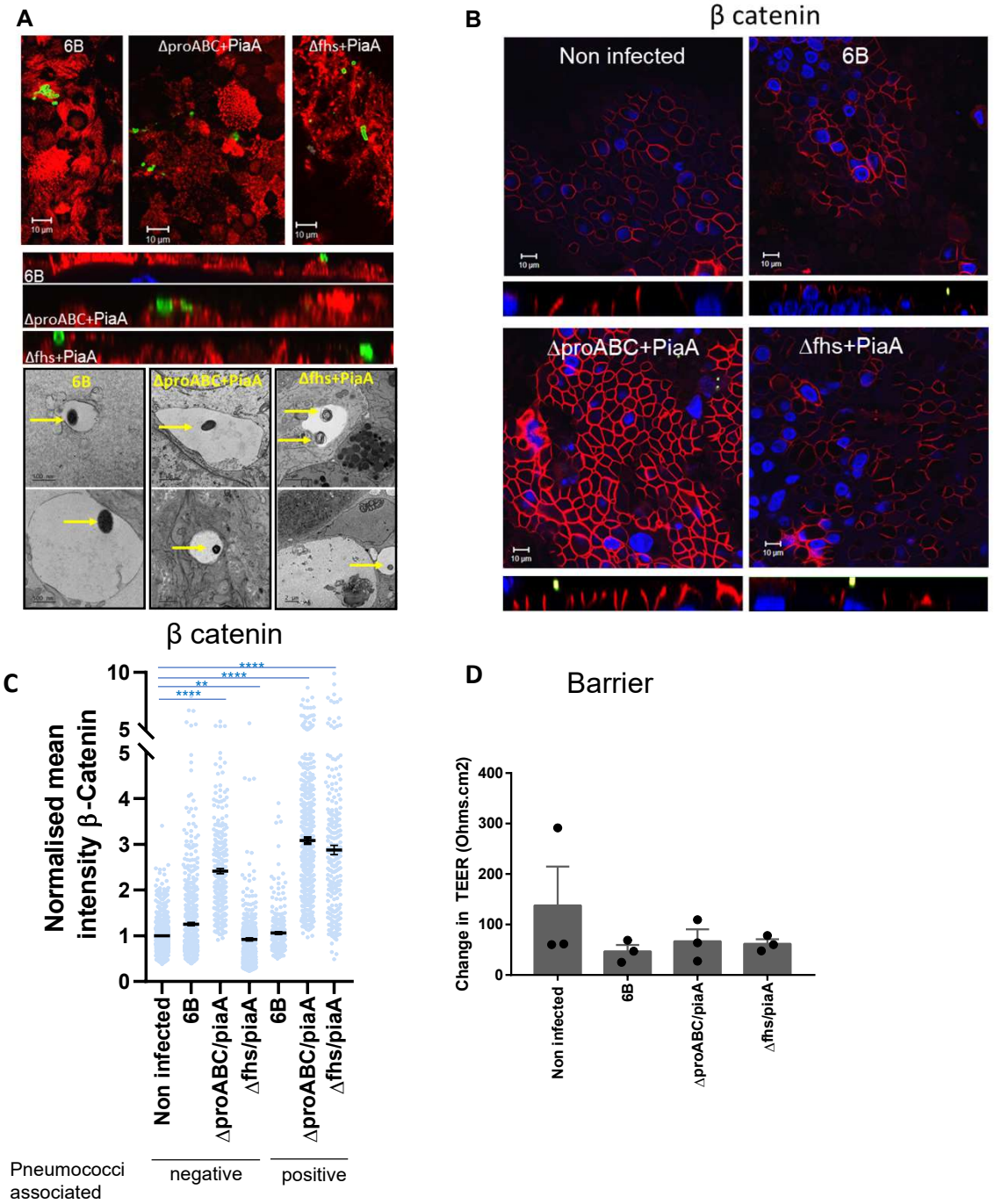

Figure 3. Pneumococcal – epithelial interactions with primary human epithelial cells.

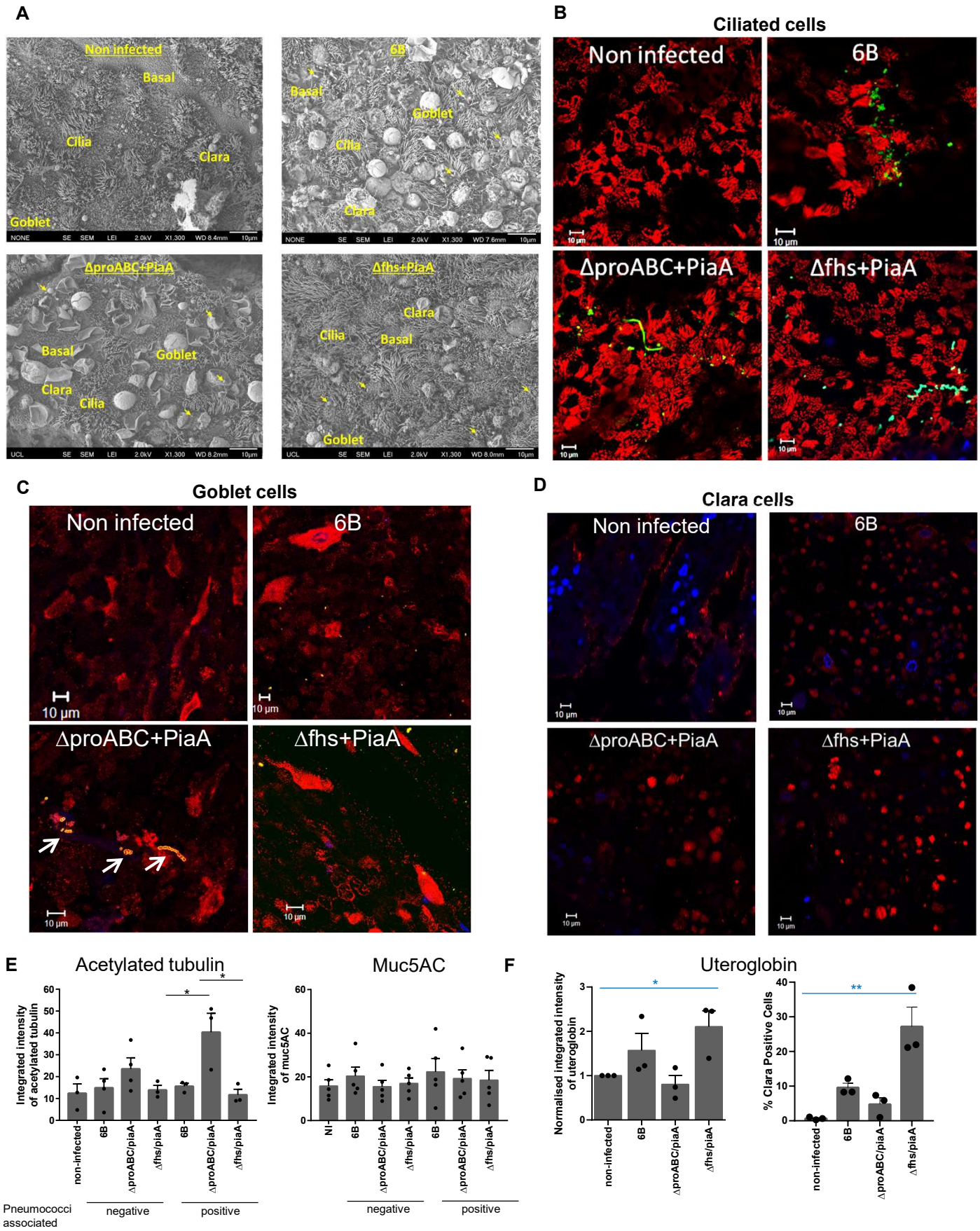

Figure 4. Strain association, microinvasion and transmigration of Detroit 562 cells.

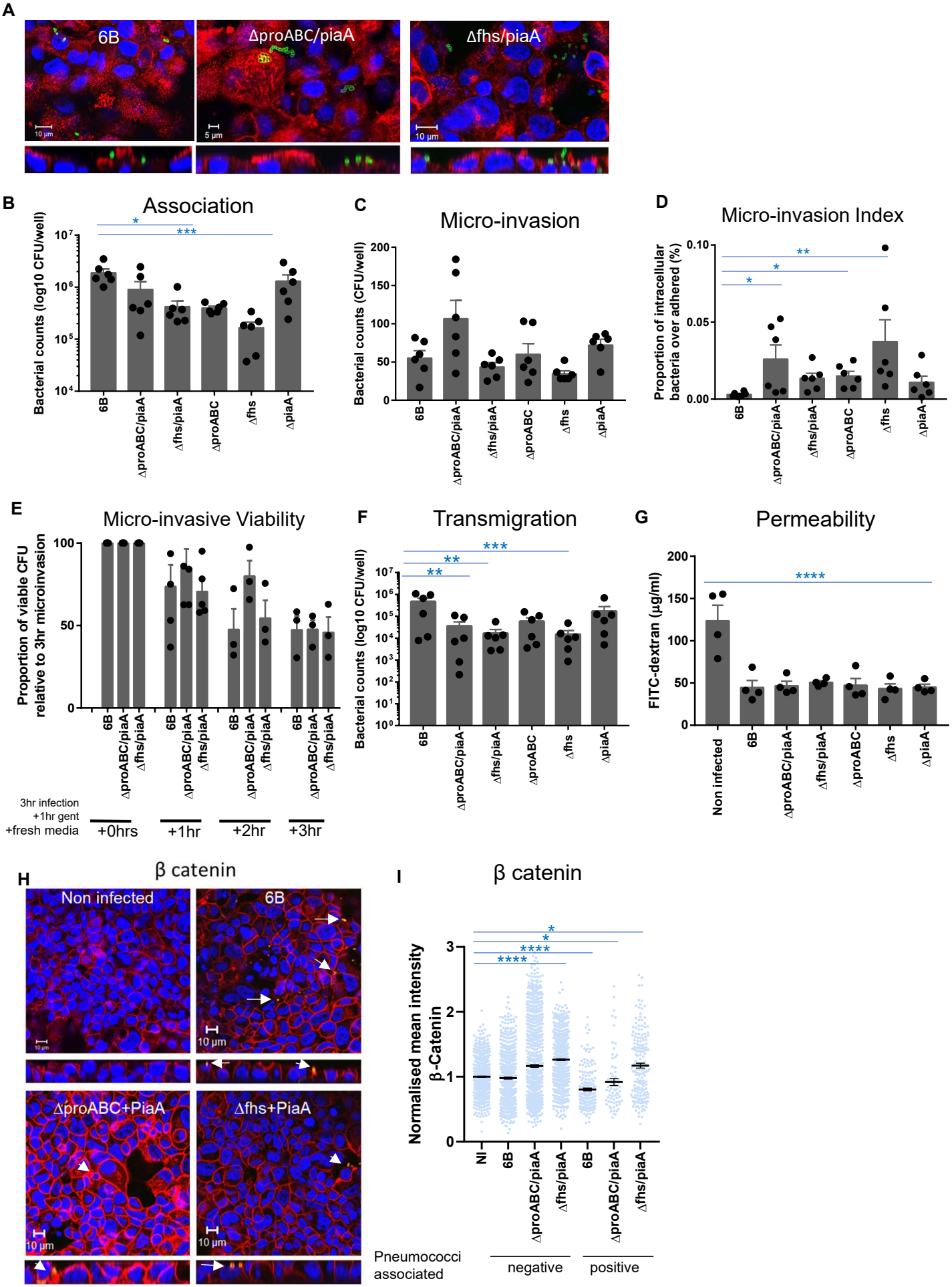

Figure 5. Detroit 562 cell transcriptomic responses to pneumococcal strains.

A

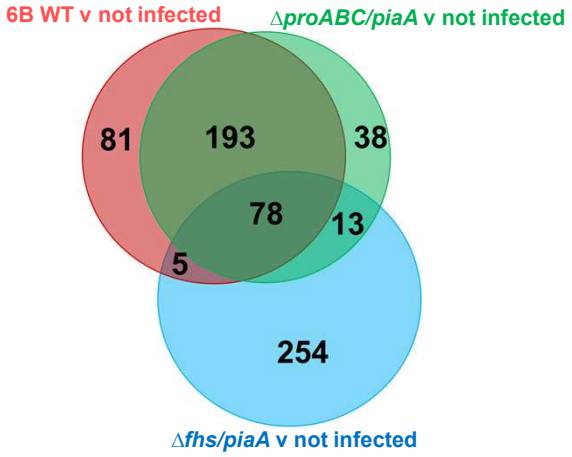

B

log2foldchange	6B	ΔproABC/piaA	Δfhs/piaA
Upregulated genes			
AC256236.1	32.9	25.5	0.0
AC022149.1	30.2	27.6	0.0
Z84488.2	29.1	21.6	0.0
MUC21	25.8	29.0	0.0
VASN	20.9	0.0	0.0
BRD2	18.4	24.7	0.0
AC012254.2	18.2	13.8	0.0
CTAGE4	18.1	0.0	0.0
MICE	17.1	20.3	0.0
AC107075.1	10.1	0.0	0.0
CSNK2B	0.0	20.2	0.0
MTRNR2L6	0.0	19.4	15.8
LSM2	0.0	17.1	0.0
ALOX5	0.0	0.0	6.9
AC006064.6	0.0	0.0	3.4
TAP2	0.0	0.0	3.2
CYP1A1	0.0	0.0	1.7
FOSB	0.0	0.0	1.4
IL1B	0.0	0.0	1.3
CXCL8	0.0	0.0	1.1
CXCL2	0.0	0.0	1.1
CYP1B1	0.0	0.0	1.0

C

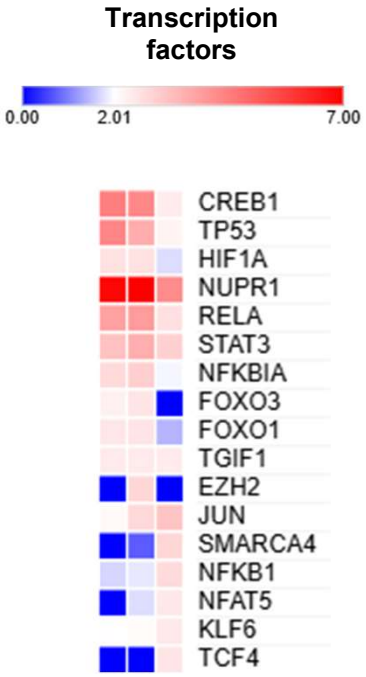

D

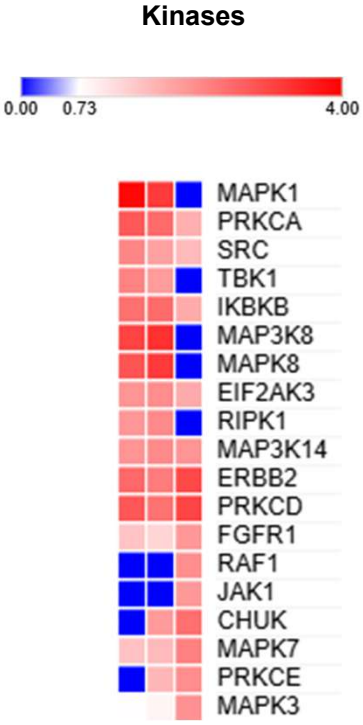

Figure 6. Effects of pneumococcal infection on caspase activity in Detroit 562 cells.

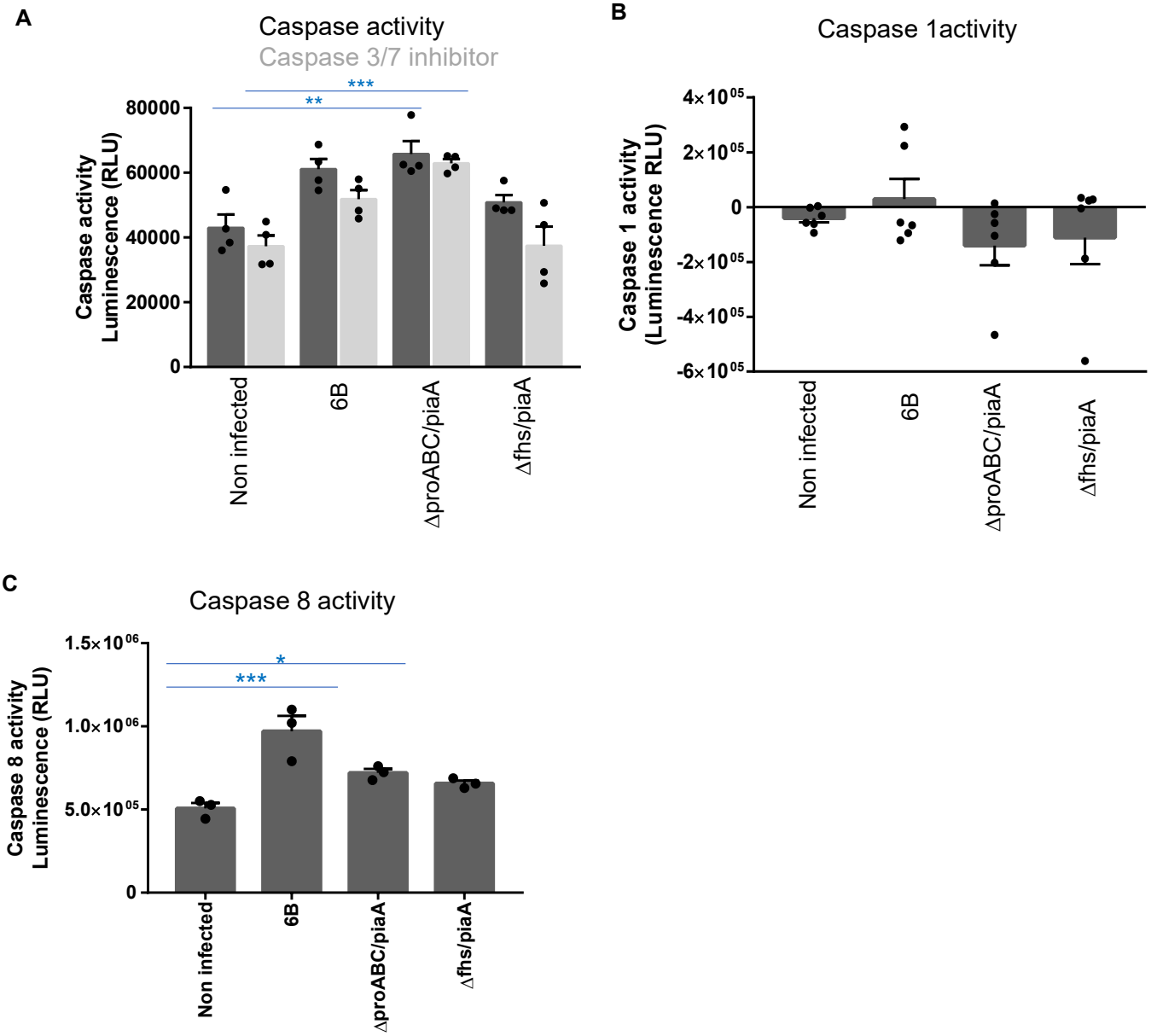

Figure 7. Hydrogen peroxide secretion and pneumolysin activity from pneumococcal strains in the absence and presence of Detroit 562 cells.

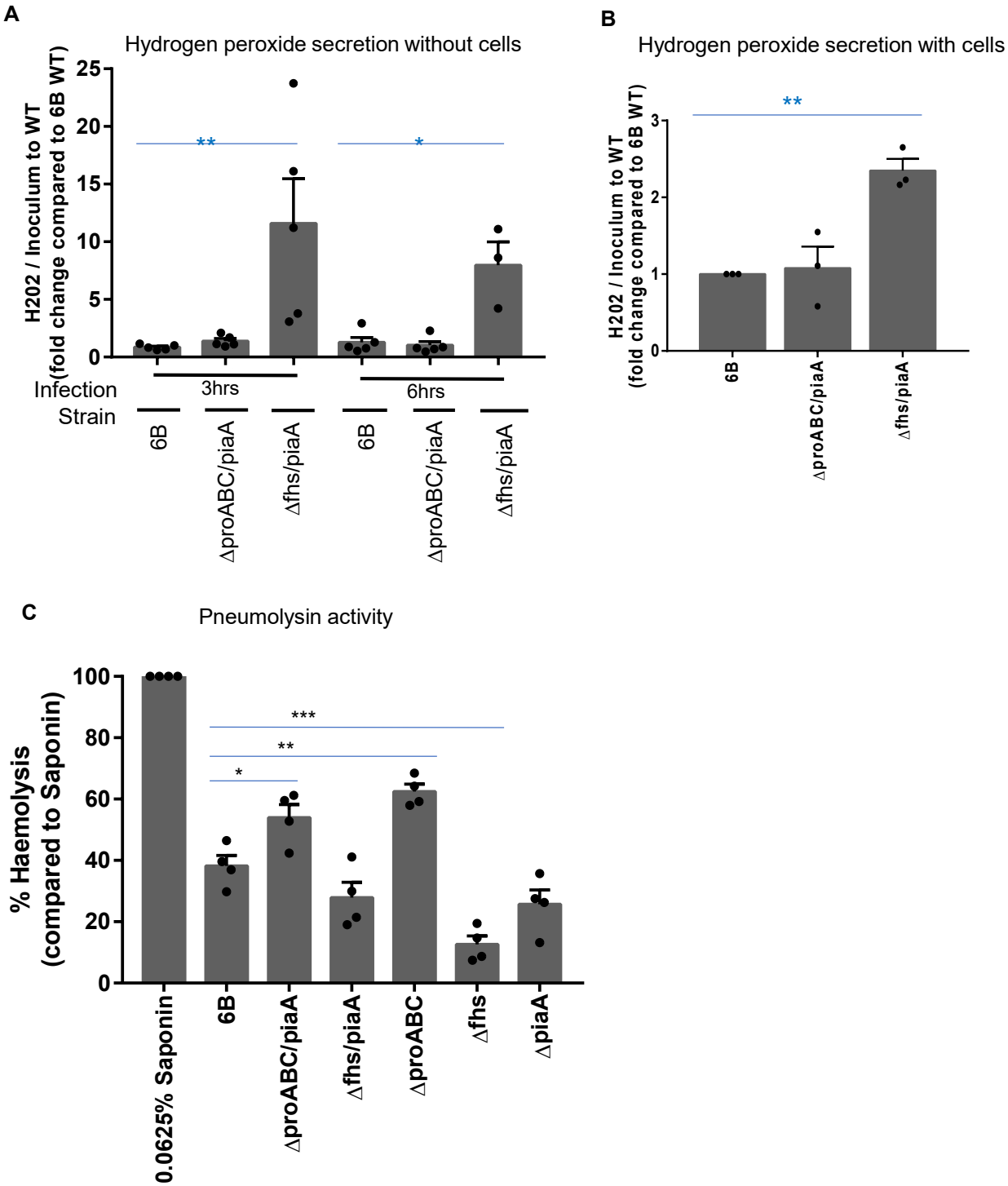
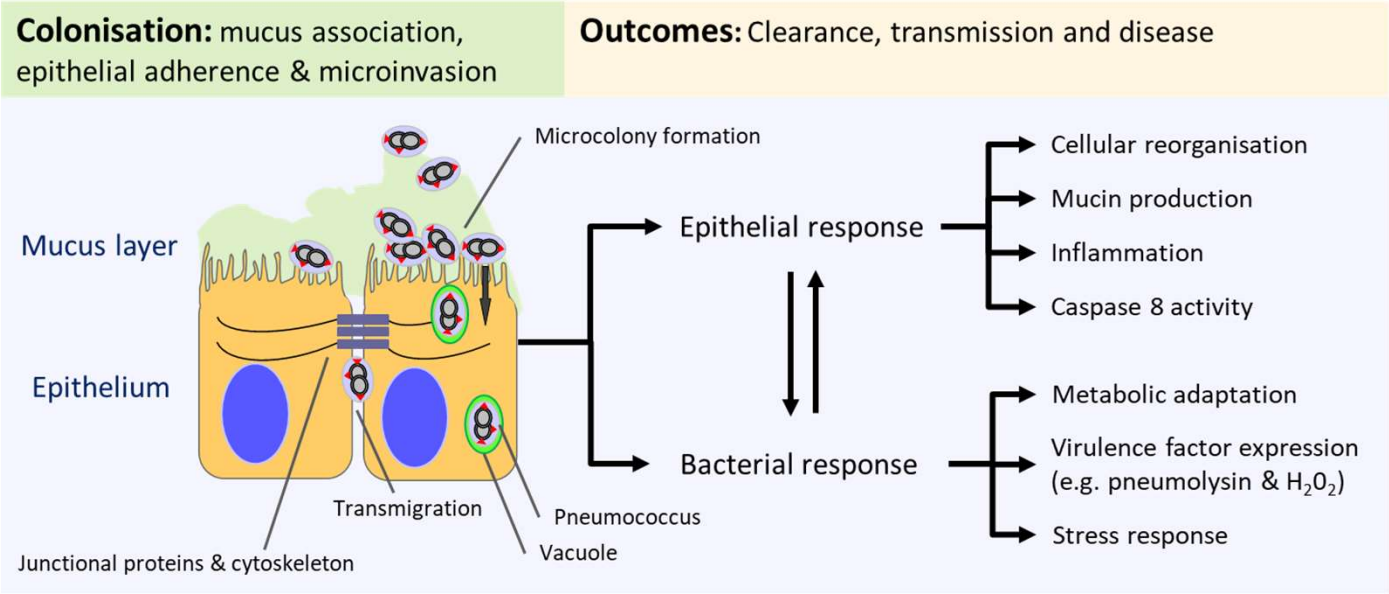
Graphical abstract